Pattern Classification of Terrain During Amputee Walking

by

Matthew Todd Farrell

S.M., Massachusetts Institute of Technology (2009)
B.A., Bard College at Simon's Rock (2004)

Submitted to the Program in Media Arts and Sciences,
School of Architecture and Planning,
in partial fulfillment of the requirements for the degree of

Doctor of Philosophy in Media Arts and Sciences

at the

MASSACHUSETTS INSTITUTE OF TECHNOLOGY

June 2013

Author_____
Program in Media Arts and Sciences
May 15, 2013

Certified by_____
Hugh Herr
Associate Professor of Media Arts and Sciences
Program in Media Arts and Sciences
Thesis Supervisor

Accepted by_____
Pattie Maes
Associate Academic Head
Program in Media Arts and Sciences

Pattern Classification of Terrain During Amputee Walking

by

Matthew Todd Farrell

Submitted to the Program in Media Arts and Sciences,
School of Architecture and Planning,
on May 15, 2013, in partial fulfillment of the
requirements for the degree of
Doctor of Philosophy in Media Arts and Sciences

Abstract

In this thesis I study the role of extrinsic (sensors placed on the body) versus intrinsic sensing (instruments placed on an artificial limb) and determine a robust set of sensors from physical and reliability constraints for a terrain adaptation in a robotic ankle prosthesis. Further, during this thesis I collect a novel data-set that contains seven able-bodied participants walking over 19 terrain transitions and 7 non-amputees walking over 9 transitions, forming the largest collection of transitions to date using an exhaustive set of sensors: inertial measurement units, gyroscopes, kinematics from motion capture, and electromyography from 16 sites on the lower limbs for non-amputee subjects and 9 sites or amputee subjects. This work extends previous work [3] by using more conditions, a larger subject group, and more sensors on amputees, and includes non-amputees.I present a novel machine learning algorithm that uses sensor data during rapid transitions from pre-foothold to just prior to post-foothold to predict different terrain boundaries. This advances the field of biomechatronics, our understanding of terrain adaptation in people both with and without amputations, contributes to the development of a fully terrain adaptive robotic ankle prosthesis, and improves the quality of life for the physically challenged. Specifically we set out to prove between pre and post-foothold the ankle and knee positions calculated using an IMU attached to an amputees powered prosthetic ankle can discriminate with greater than 99% accuracy between 9 conditions. Our results suggest that myography as a non-volitional sensing modality for terrain adaptive protheses was not needed.

Thesis Supervisor: Hugh Herr
Title: Associate Professor of Media Arts and Sciences, Program in Media Arts and Sciences

3

Pattern Classification of Terrain During Amputee Walking

by

Matthew Todd Farrell

The following people served as readers for this thesis:

Thesis Reader_____

Rosalind W. Picard
Professor of Media Arts and Sciences
Program in Media Arts and Sciences

Thesis Reader_____

Joeseph Paradiso
Associate Professor of Media Arts and Sciences
Program in Media Arts and Sciences

Contents

List of Figures

List of Tables

Chapter 1

Introduction

1.1 Executive Summary

Modern ankle prostheses are still very simple devices. Only very recently have they incorporated more advanced control strategies to adapt to varying walking speed and minor slope changes. This work makes them more useful on a wider range of terrain. However, a major question in the field of robotic prostheses is how to go about designing a practical interface for a robotic prothesis. A major limitation of previous studies in this space is the lack of available data on how subjects behave during walking – amputee subjects are difficult to find and recruit for demanding studies. Further, the use of particular sensors do not often make sense.

Electromyography, and other extrinsic sensing, has long been assumed to be useful

since it measures aspects of an amputee's physiology. Indeed this could be true, but for practical purposes EMG can often be quite difficult to use for the measure of repeatable muscle activations and has seen limited product application outside of upper-limb prostheses. Intrinsic sensors are much easier and have well-understood mechanical components that make them more ideal as a long-term solution, but will they work as well as electromyography and other externally worn sensors?

Below-knee amputees still face problems when navigating varying terrain; they risk falls during rapidly changing terrain. The existing solutions that allow people to change the mode of their prostheses tend to encumber the user, and are difficult to use on a daily basis. To solve this problem prosthesis designers have focused on using a simpler set of sensors to achieve terrain adaptation.

In this thesis, I present an algorithm that uses biological data from able-bodied subjects, and determines the best set of sensors and features for terrain adaptation when amputees are wearing a robotic ankle prosthesis. The novel data-set consists of subjects with intact limbs and subjects with a below-knee amputation wearing a robotic prosthesis. Each dataset contains information obtained from 16 channels of electromyography (EMG), gyroscopes, inertial measurement units, pressure, and kinematic motion from motion capture on 19 different types of transitions for non-amputees and 9 transitions for amputees. Then 11 features are extracted from each channel that result in the final training data-set, that contains a total of 290 features for non-amputee subjects and fewer for amputee subjects, with between 100 and 200

features (depending on the number of available muscles). These data are then run through a pattern recognition algorithm utilizing a Naive Bayes classifier with an uninformed prior, and then sequential floating forward search is applied to the training matrix. For each subject, the algorithm results in the best set of features to accurately determine the terrain underneath the foot (right before foot-fall on the opposite side of a terrain change). Then these results are compared against the results of other methods.

Specifically we set out to prove that between pre- and post-foothold the ankle and knee positions calculated using an IMU attached to an amputees powered prosthetic ankle can discriminate with greater than 99% accuracy between the following 9 conditions:

1. level ground and a 15 degree incline,
2. level ground to a 15 degree decline,
3. 15 degree incline to 15 degree decline,
4. 15 degree incline to level ground,
5. 15 degree decline to a 15 degree incline,
6. 15 degree decline to level ground
7. level ground to stair descent,
8. level ground to stair ascent,

9. level ground without incline or decline.

If the ankle is transitioning between two terrain types that vary less than 15 (degrees) then the passive compliance of the ankle should be able to manage the terrain and produce the appropriate amount of power.

The design specifications of the algorithm were determined by the need to solve two particular problems: robustness and ease of use. Robustness, for this thesis, is defined as when the classifier has $\geq 90\%$ accuracy in identifying the terrain underneath the foot. The features are chosen to be the most robust, with the particular classifier chosen, for that particular subject, or, in indicated cases, with multiple subjects.

We evaluate these features, after we have decided which sets product above 95% accuracy, to see which ones are the least invasive. The most invasive are those features which belong to sensors that are placed directly on the body like EMG, a button, camera, sound sensing, and those that are least invasive are those that are a mechanical component of the prosthesis.

To evaluate the algorithm, we will evaluate the classifier's performance on the data collected in a series of experiments with both non-amputee and amputee participants. Each amputee will be wearing a robotic or passive prosthesis. Finally, these data are evaluated to discover the role of EMG sensing in below-knee amputees.

This research has been approved by the MIT Committee on the Use of Humans as Experimental Subjects (COUHES). Each experiment consists of one approximately five

hour session during which subjects are asked to traverse 19 unique terrain transitions while wearing the suite of sensors described above.

My dissertation improves our understanding of how terrain adaptation takes place in humans and how to apply these principals to bionic systems. These objects are poised to improve the lives of people living with disabilities.

1.2 Introduction

In the United States alone, there are 1.7 million people living with a leg amputation (NLLIC, 2008). In addition, each year there are 134,000 new amputations in the United States and 30% (40,200) of those are below-knee amputations (Adams, 1999, Ziegler-Graham, 2008). The loss of a limb causes several health problems that can be traced to an amputee's relative lack of mobility. This includes an increased risk of falls, stumbles, and injuries arising from these varying terrain. While recent advances, most notably robotic prosthetic ankles, can improve metabolic economy and produce a biomimetic gait, the state of the art cannot adapt to a wide variety of changing terrain conditions robustly.

Most robotic prostheses incorporate a computerized controller, so that users can walk on even terrain. These prostheses provide power while walking up and down very small grade ramps that are typically less than 8.5 degrees. Innovations, like those

mentioned, and the use of embedded computers make complicated locomotion tasks more tractable.

Intrinsic control in a robotic prostheses takes sensor information from the internal sensors (sensors that compose a mechanical part of the robotic ankle) to control the behavior of the ankle during a typical gait cycle. An intrinsic sensor can be thought of as, "a sensor that measures the state of the robotic ankle and provides torques to the joint in response to the environment." *Extrinsic control*, on the other-hand, is usually something apart from the prosthetic limb and measures physiological properties of the body. For example, people measure things like electrical properties, non-affected limb joint angles, and their positions in space, using sensors attached to the non-robot part of the body.

Currently, users with extrinsic controls can manually change the mode of their prosthesis at the cost of a relatively non-intuitive interface [8]. A button or switch is too cumbersome for biomimetic terrain adaptation. For example, non-amputees do not have to stop and press a button to change locomotion modes. I want to address this problem so that the algorithm described in this thesis can utilize a group of sensors attached to an instrumented limb to discover how able-bodied subjects smoothly transition between terrain modes. Then from these sensors, I pick the sensors that are minimally invasive for the user and will stand up to daily wear.

I take insights from biomechanics and machine learning to find the "best" set of

sensors and features for terrain adaptation. In particular, I get the set of sensors I need to accurately and robustly determine the type of slope underneath the foot at the most critical moments during locomotion. The sensors are either placed on the body of the amputee (extrinsic), or they are a physical part of the robotic limb (intrinsic). From each individual sensor there is a data stream that is analyzed by the algorithm which is developed in this thesis. It reveals the nature of biomimetic terrain adaptation using real internal measurement unit (IMU) data collected from a robotic ankle during locomotion.

I end the thesis with a discussion of how this algorithm could be used to control the behavior of a powered-ankle prostheses for terrain adaptation using real IMU data collected on a robotic ankle during locomotion. I also make suggestions based on the results of the algorithm I developed, and talk about the specific minimal set sensors that are needed for each subject. Finally, I will cover the improvements that could be made to the algorithm and make suggestions for future work.

Specifically we set out to prove that between pre- and post-foothold the ankle and knee positions calculated using an IMU attached to an amputees powered prosthetic ankle can discriminate with greater than 99% accuracy between the following 9 conditions:

1. level ground and a 15 degree incline,

2. level ground to a 15 degree decline,

3. 15 degree incline to 15 degree decline,

4. 15 degree incline to level ground,

5. 15 degree decline to a 15 degree incline,

6. 15 degree decline to level ground

7. level ground to stair descent,

8. level ground to stair ascent,

9. level ground without incline or decline.

If the ankle is transitioning between two terrain types that vary less than 15 (degrees) then the passive compliance of the ankle should be able to manage the terrain and produce the appropriate amount of power.

Chapter 2

Background

2.1 Related Previous Literature

Recently, robotic prostheses for the lowerlimbs have been shown to improve the efficiency of level-ground walking [5]. These prostheses incorporate computerized control and can assist users with level-ground walking. The use of embedded computers makes complicated locomotion tasks tractable by allowing more powerful control algorithms to be used during movement. Most robotic prostheses take sensor information from internal sensors (sensors that are located on the prosthesis) to control the behavior of the ankle during a typical gait cycle – this is called intrinsic control. Less frequently, a robotic prosthesis can take information from external sources of information for control algorithms – this is called extrinsic control.

Currently, users can change the mode of their prosthesis manually at the cost of a relatively non-intuitive interface [8]. We feel that these interfaces are too cumbersome for biomimetic terrain adaptation. An interface that requires the user to stop and start when they want to change their mode of locomotion or stare at their hands during movement is never going to be as efficient as human locomotion adaptation. Our solution is to develop a robotic prosthesis that can utilize a group of sensors attached to an instrumented limb to smooth transitions between terrain modes.

Electromyography (EMG) has been used in upper-limb prosthesis control for decades[9][10][11][12]. It is the primary neural control input to the majority of robotic upper-limb prostheses. It has been shown to be effective when used with pattern recognition algorithms that infer the intention of the user. More recently, the desire to make lower-limb prostheses that can adapt to terrain in a biomimetic way has spurred interest in using neural signals as a control input. Very recently, a pattern recognition method for identifying locomotion modes from EMG has been developed[3]. The results suggest that the thigh muscles of a trans-femoral amputee might be sufficient to obtain reasonably accurate identification of terrain during steady-state walking, but they concluded that classification with EMG alone may not be sufficient for robust classification of different locomotion modes. Earlier work by Praeer et. al. [7], show that there is a difference in EMG envelope, which suggests that hip-muscles might be useful in discriminating different locomotion modes. Huang et. al [3], also observed this and developed a system around it capable of discriminating different user-modes.

However, the author of this study did not select those features of the EMG signal that were the *most* useful. In 2006, Jin et. al. [6] developed an algorithm that identified terrain during level-ground walking. However, the features were extracted from one entire gait-cycle, which would make implementation in a real-time system dangerous; the delay introduced by waiting one whole gait-cycle to determine terrain can easily lead to falls. Farrell, et. al. [13] reports that an optimal controller delay for upper-limb prosthesis is between 100ms and 125ms, and there is a linear performance degradation as the system delay is increased. Based on the previous work, it is our opinion that a strategy that employs very fast updates should be used to identify user locomotion modes on varying terrain.

The EMG signal is difficult to use for locomotion mode discrimination; it is time varying and the features of the signal change within the same task over time. In order to quickly discriminate between locomotion modes, the electromyographic recording of each task needs to have a repeatable difference that can be observed by a collection of features. Using a larger window can increase the amount of information available for decision making with a pattern recognition algorithm. However, by using a larger window it is possible that features between two modes might overlap and decrease the accuracy of a pattern recognition algorithm, so instead we used short windows (200ms) to extract EMG information. This was observed between toe-off and heel-strike during some trials in [3].

Until a reliable form of neural-control is developed, robotic prostheses will likely use

data-fusion [14], incorporating sensor information from a variety of sensors, to determine the type of terrain the user is walking over. Without a good feature selection algorithm it would be impossible to develop a robust data-fusion algorithm that can estimate terrain. More specifically, a data-fusion algorithm uses the features of a signal to estimate the state of the robotic-ankle prosthesis continuously. For the data-fusion algorithm to track variables continuously, or discriminate between locomotion modes, the features should have strong discriminatory power. In this work, we take the first step in developing a data-fusion algorithm by first understanding which features of both EMG and other internal sensors are useful in discriminating between locomotion modes.

Outside of EMG there are a large range of sensors that can be used, and that are placed directly inside a lower-limb prostheses. Many studies have used accelerometers, gyros, strain gauges, and goniometers to infer the state of the ankle in the real world (see [17] and references within).

Our approach, in this thesis is to use a wrapper-based feature selection algorithm with sequential feature selection methods[15] to focus on those features and muscles that provide the lowest-error classifiers for two trans-femoral amputees and one trans-tibial amputee. Hargrove, et al. [2] have used similar approaches for upper-limb prostheses. The researchers successfully used uncorrelated linear discriminant analysis (ULDA) to discriminate between movement classes in upper-limb prostheses. Their results suggest that using several different classifiers that train between several pairs of

different tasks might be more practical than building one classifier for all classes. Later work [3] showed it is possible to extract large amounts of neuromuscular information from electromyography from windows at important points of the gait cycle. However, in previous work no one has picked out the particular features of the lower limbs that are mostly responsible for classification accuracy. Our work builds off these two studies and develops a novel feature selection method that can be used with above-knee and below-knee amputees, and that directly attribute classification accuracy with specific features. Specific results concerning both groups are discussed alongside ways to improve this method.

2.2 Biomechanics Background

2.2.1 Electromyography (EMG)

Starting largely with the development of upper-limb prostheses, researchers realized that myographic signals from residual muscles can be used to improve the ability of grasping in single-degree of freedom robotic hands. In 1972, Woodie Flowers explored the use of proportional myoelectric control in a pneumatic robotic knee [1]. Since then bioelectric signals have been used less frequently than mechanical sensing from the actual prosthesis. This was the result of advances in microelectronics and computing power at a small scale – the use of accelerometers, small circuit boards, etc, all con-

tributing to the relative abandonment of bioelectric sensing in lower-limb prostheses. In addition, since quality of life and comfort is so important, adding sensors to the body incurs a cost.

Advances in the myoelectric and neural control of upper-limb prostheses brought about interest in the possibility of controlling lower-limb prostheses using bioelectric signals [2]. Most of the advanced control frameworks for upper-limb prosthesis control have used pattern recognition to find control signals. Hu and Hargrove [18][2] have written good reviews of pattern recognition techniques for myoelectric systems that detail the use of upper-limb prostheses.

The typical physiological signals used for the control of lower-limb prostheses are electromyographic (EMG) signals recorded either inside the muscle, or on the surface of the skin, or internally with IMES (Implantable Myoelectric Sensors) [21]. However, it is less practical because it requires surgeons to implant the electrodes and usually a special battery powered receiver needs to be wound around the socket, and non-invasive signals can be obtained from an electrode placed on the surface of the skin close to the muscle belly. While this does increase the delay, until the surgery is more common-place it's use is suspect.

More recently, Professor Loeb at USC, [21] has developed Internal Myoelectric Sensors (IMES) to measure EMG at the muscle-implanted location of the electrode. The value of this technology being that, "the distance from the site of motor unit activation

matters, so IMES readings should be more accurate and less noisy than traditional surface EMG."

Minimizing the noise in EMG is very important and system developers need to understand how sensitive their systems are to variance and changes in the underlying EMG signal. Hogan and Clancy [19] developed the first mathematical models of EMG that used the amplitude of the signal as a rough estimate of force produced by the muscle. The amplitude is often used as a control input for upper-limb prostheses, while for lower-limb prostheses, surface EMG is used [5] for control of plantar flexion of their devices. Note that the algorithm needs training and frequently requires re-training to use properly [5].

Ferris [20] also uses amplitude as an approximation of muscle motor unit recruitment for plantar flexion of the ankle. This strategy, called proportional myoelectric control, is the oldest and perhaps most widely used control strategy because it is also the simplest [19][11]. However, many more complicated representations of the EMG signal have been used over time [18]. In most of these cases a typical EMG controlled system will be composed of a collection of electrodes, amplifiers, filters, software for feature extraction and classification, and a controller to servo the prosthesis into position, see Fig2-1 below.

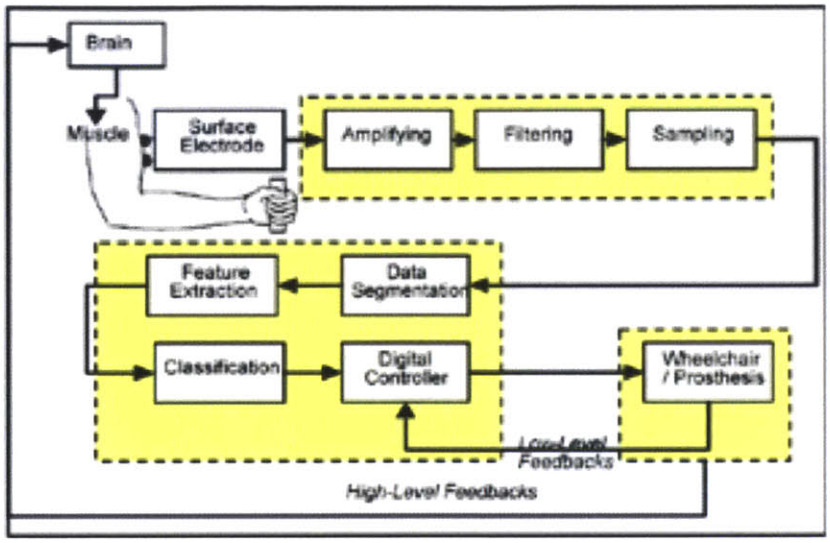

Fig. 1. A myoelectric control system based on pattern recognition.

Figure 2-1: Many control systems that are based on electomyography tend to present a very similar structure. This structure replicates a hypothetical EMG control system that would be developed from this work. This thesis focuses primarily on parts extending from the *surface electrode* to the classification of the signal into a category that can be used in a controller.

2.3 Intrinsic Signals Background

2.3.1 IMU/Gryoscope Background

With the miniaturization of electronics have come wearable Inertial Measurement Units (IMU). An IMU is typically composed of an accelerometer and/or gyroscope and has been used for applications such as counting steps, measuring stride length, or detecting changes in acceleration [22]. IMUs have also been used in measuring changes in angular velocity [23][24], a single IMU may be a reliable enough to accomplish these things.

However, lower-limb prostheses that will work with terrain adaption might require several IMUs on the body. In particular, for detecting transitions between different terrains it might be impossible to use a single IMU without some other type of intrinsic sensing or a fusion of extrinsic sensing. The literature is not clear on this last point and only recently [3] have fusion algorithms started to show up that use both intrinsic and extrinsic sensing for terrain adaptation.

IMUs pose some challenges. The reason for using an IMU is to know something about the forward velocity of a limb, the orientation of the body in space, or the position of the IMU relative to some fixed position. All of these things require the device to integrate the accelerometer data up to the velocity or the position. This means that errors are incorporated into the estimates for velocity and position can cause drift in the measurements. However, it is possible to use information from other sensors to correct for this drift. In particular, exploits magnetometers and knowing the timing of heel-strike can correct for drift by combining measurements in a Kalman Filter.

Correction to integration errors of IMUs for gait is well understood. In fact, it is possible to obtain absolute estimation of ambulatory foot orientation and position using accelerometers and gyroscopes, with force sensors that detect foot-ground contact and force [24]. This works because the foot is approximately at rest and directly on the ground during foot-flat, no matter the type of surface. This resets the bounds of integration to be reset during cyclic-walking [25][26].

Chapter 3

Sensor Selection Algorithm

The sensor selection algorithm described in this thesis combines several different areas of machine learning to make a prediction about which feature/sensor combination will produce the most powerful combination of sensors that will perform best on actual clinical data. For a graphical representation see Figure 3-1.

3.1 Wrapper-based Feature Selection

The goal of the sensor selection algorithm is to reduce the number of sensors a patient has to wear during the daily usage of their device. Wrapper selection methods provide a way to do this by searching through a collection of features and measuring them against a cost function. The cost function in our case is Naive Bayes with cross

validation. There are many different types of wrapper-based search available [15], and an infinite number of cost functions that can be used with each of these selection methods.

The sensor selection algorithm uses sequential-forward-search (SFS) and sequential-floating-forward-search (SFFS). These are very basic algorithms, and while there are more advanced selection algorithms available, these are very powerful – the sensor selection algorithm reduced the number of features by as much as 98% – this is clearly powerful enough to do a good job with our data at hand. More advanced methods[29] do exist, but depending on the type of training matrix the performance of each of these algorithms can vary widely – there is no optimal feature selection algorithm for all training sets.

During SFS and SFFS the best performing features will be those that produce very accurate measurements of the terrain. Later in this thesis, we study which objective function will perform best with SFFS or SFS, since we are trying to maximize classification rate.

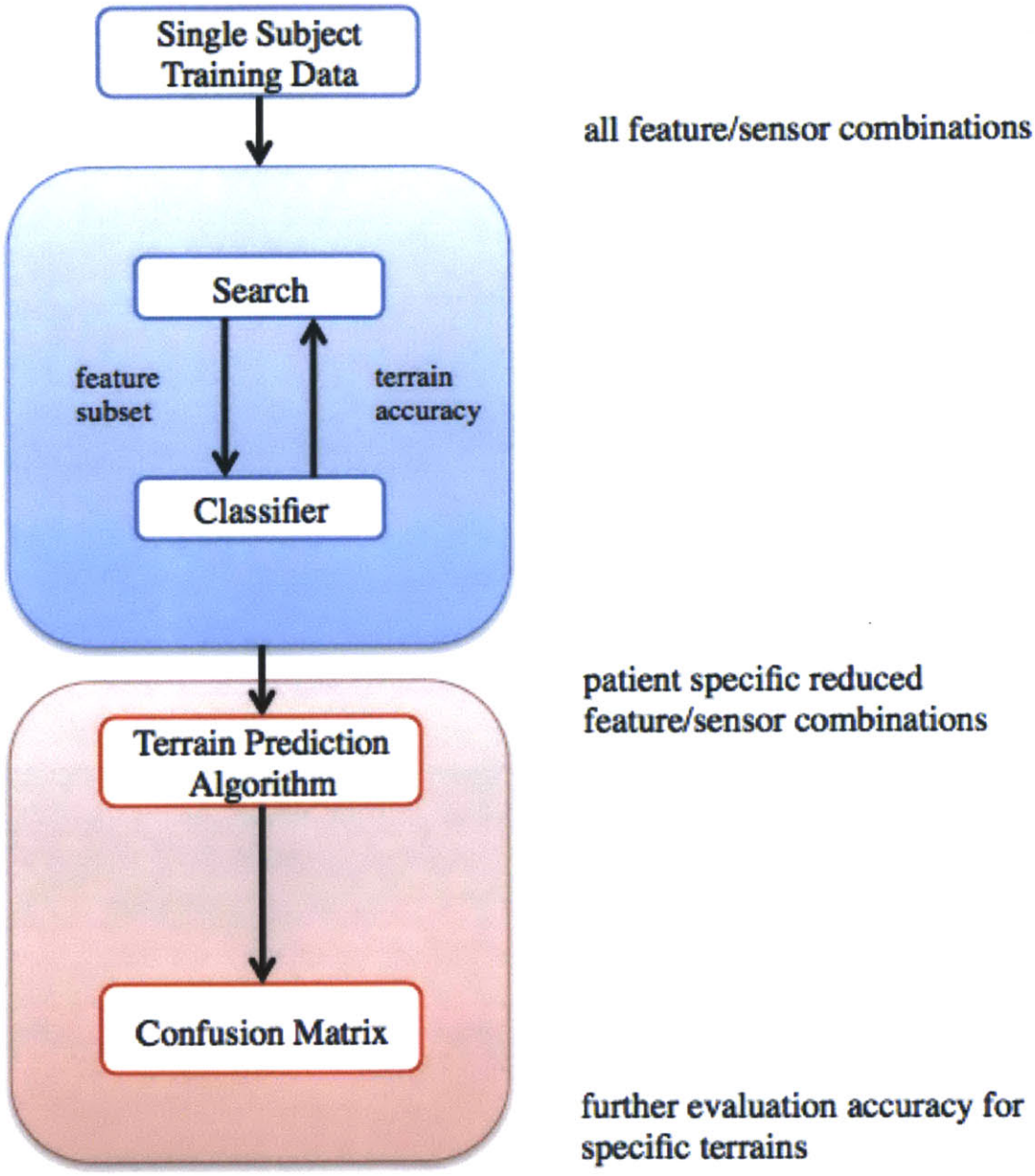

Figure 3-1: The sensor selection algorithm.

3.1.1 Theoretical Framework – Feature Extracting Algorithm

3.2 Terrain Classification

Phase-dependent Naïve Bayes Classifier

The phase-dependent classifier was introduced in [3] to account for the non-stationary behavior of EMG over time and increase the responsiveness of the system. The windows are placed near important times in the signal. Typically the location where it would make sense to encounter strong muscle contraction is during loading of the limb. The majority of muscular information is likely to be present in the extrinsic and intrinsic signals primarily during stance and near the beginning of swing.

Classifiers that use longer time windows are subject to continual changes in the EMG signal. The phase-dependent classifier relies on the quasi-cyclic nature of the EMG signal at these key moments in the gait cycle. At these points the signal has low-variation in the second order moment of the signal, is quasi-stationary, and repeatable at the same time in the gait-cycle. This benefits any classifier that uses the statistics of the signal to perform pattern recognition.

The *naive bayes classifier* is a simple probabilistic classifier that makes strong assumptions about the independence of the features – essentially, it is an independent feature model. Mathematically, given a terrain of type, T, and a feature vector

$\mathbf{X} = (X_1, \ldots, X_n)$ we have likelihood of the data as,

$$P(\mathbf{X}|T) = \prod_{i=1}^{n} P(X_i|T).$$

The decision rule to assign a particular terrain to sample is derived by the following argument. Given that we do not know the frequency at which a certain terrain will appear we can use an uninformed prior,

$$P(T_1) = \frac{1}{n} = P(T_2) = \ldots = P(T_n).$$

From this we model the decision rule is the maximum a posteriori that picks the most likely terrain given a sample,

$$\arg\max_{T_i} P(T_i|\mathbf{X}) = \arg\max_{T_i} \frac{P(\mathbf{X}|T_i)P(\mathbf{X})}{P(T_i)}.$$

By assmption, $P(T_i) = \frac{1}{n}$ for $i = 1, 2, \ldots, n$. This mean that $P(T_i)$ and $P(\mathbf{X})$ can be factored out of the maximum that results in decision criteria becoming,

$$nP(\mathbf{X}) \cdot \arg\max_{T_i} P(\mathbf{X}|T_i) = nP(\mathbf{X})) \cdot \arg\max_{T_i} \prod_{i=1}^{n} P(X_i|T_i),$$

which gives

$$f(T_i) = \arg\max_{T_i} \prod_{i=1}^{n} P(X_i|T_i)$$

where this final decision criteria form is obtained by combining this derivation with the expansion of the likelihood in terms of terrains.

This assumption is highly unrealistic since the majority of features are related in complicated ways. The success of the method is largely due to the nature of optimality in terms of the zero-one (loss see http://www.cc.gatech.edu/ isbell/reading/papers/bayes-opt.pdf) which does not require a high-fidelity model of the probability distribution. The optimal classifier is obtained as long as the actual and estimated probability distributions agree on the most likely class[27].

For trans-tibial amputees, the window was much smaller (on average 0.6 sec) for just the transition. This was largely due to the nature of a transition between terrain. In particular our participants transitioned very quickly between terrains, so it is possible that a slower transition speed could produce better results with EMG-based features. The mechanical sensors, for simplicity, were also sampled in a window that had the same length as the EMG analysis window. Mechanical sensors typically have less variance than EMG, so this window-length should be sufficient for the purpose of classification.

Pre-Foot Hold/Post-Foot Hold and Heel-Contact Toe-Off Windows for a Trans-tibial Amputee

Analysis windows, as mentioned above, are usually taken around the times where the most muscular information is likely to be available. The standard configuration uses the toe-off and heel-contact points to extract musculo-skeletal information for terrain identification. We believe it is better to determine the type of terrain before an instrumented leg comes into contact with the terrain.

Transitions between terrain, in the standard window setup without pattern classification or predictive algorithms, would cause the ankle to fail. An example of this is given in Figure 3-2.

In this work, the analysis window is taken when the instrumented leg lifts off the ground and ends right before the heel hits the ground. This is assuming there is enough time to servo into the correct position, on the final terrain. In this way, the instrumented leg knows nothing about what the un-instrumented leg experiences on the first part of the terrain. In Figure 3-2, this analysis window occurs during up-ramp, so that it does not effect the classifier for the opposite side, in this case down-slope.

To test this algorithm, it needed to be verified using actual data collected from amputees and non-amputees walking over a variety of terrains.

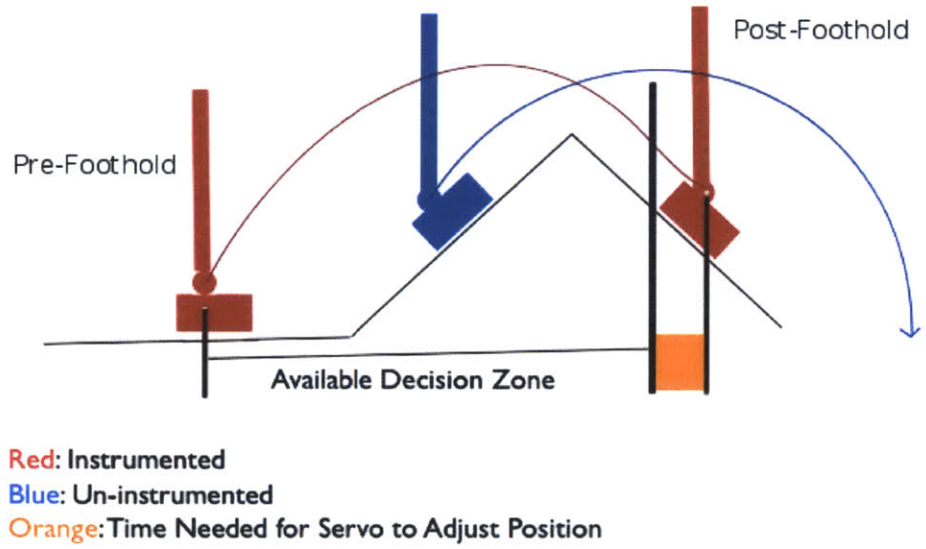

Figure 3-2: If the instrumented leg (red) does not encounter the up-slope ramp with a high-peak and has to adapt to a down-slope current IMU based algorithms and the standard window method will fail.

Chapter 4

Clinical Study 1 - Non-Amputee Subjects

In the first of three studies are to be discussed a study involving the collection of sensors and transitions from non-amputees, then amputees wearing a BiOM, and finally a smaller study with amputees and a conventional prostheses will test the feasibility of the approach described in Chapter 3. Summarized in the following table, we ran the following studies,

- Clinical Study 1 - Non-amputee Study: A total of seven participants with intact limbs walked over 19 different terrain
- Clinical Study 2 - Amputee with Robotic Ankle: This study have a total of sever participants walking over a total of 9 terrain types.

Subject ID	Age	Weight	Height
S1	28	190	5' 11"
S2	36	208	6'
S3	41	180	5' 10"
S4	33	142	5' 9"
S5	53	190	6' 2"
S6	26	170	5' 11"
S7	35	135	5' 11"

Figure 4-1: The physical characteristics of the non-amputee subjects that were included in this study.

- Clinical Study 3 - Amputee with Conventional Prosthesis: This study had 3 amputees using conventional prostheses walking over a total 9 terrain.

4.1 Participants

During this study we recruited a total of seven non-amputee participants. Our method of recruitment was to use flyers around campus advertising the study. Study participants were free of musculoskeletal injuries and could walk over each terrain normally. After the study each participant was compensated for their participation. A list of the physical characteristics of each participant is in Table 4-1.

4.2 Methods

The purpose of this study is to understand the roles of intrinsic (IMU) and extrinsic (EMG) sensors non-amputee subjects use to predict terrain with 99% accuracy. After

we have understood which features are valuable we find the features that perform up to the 99% threshold. Then we use that to influence how we evaluate the results with a robotic ankle prosthesis and later describe future directions this work can influence.

The seven non-amputee subjects listed in Table 4-1 have participated in these ramps trials. The ramps were built out of wood and placed in the motion capture area and comprised 19 different transitions, Figure 4-2. Then participants were asked to walk over the ramps (5 times per transition). Note that in each case the particular features that result in robust classification vary, see Table 7-12. However, the algorithm picks out those features which maximize the difference between particular classes through a greedy search of the features that in this case was sequential floating forward search.

In the examples of feature spaces, the different classes (depicted with different colors) tend to cluster in one region. This suggests that this method maximizes the differences among clusters and visually confirms the algorithm is finding the correct features, Figure 7-12.

From the feature spaces for each subject it is evident, even though none of these are 100% accurate with only three features, that some transitions are closer together in three-space than others. While it might be the case that each cluster is farther apart in higher-dimensional spaces a qualitative inspection is not possible.

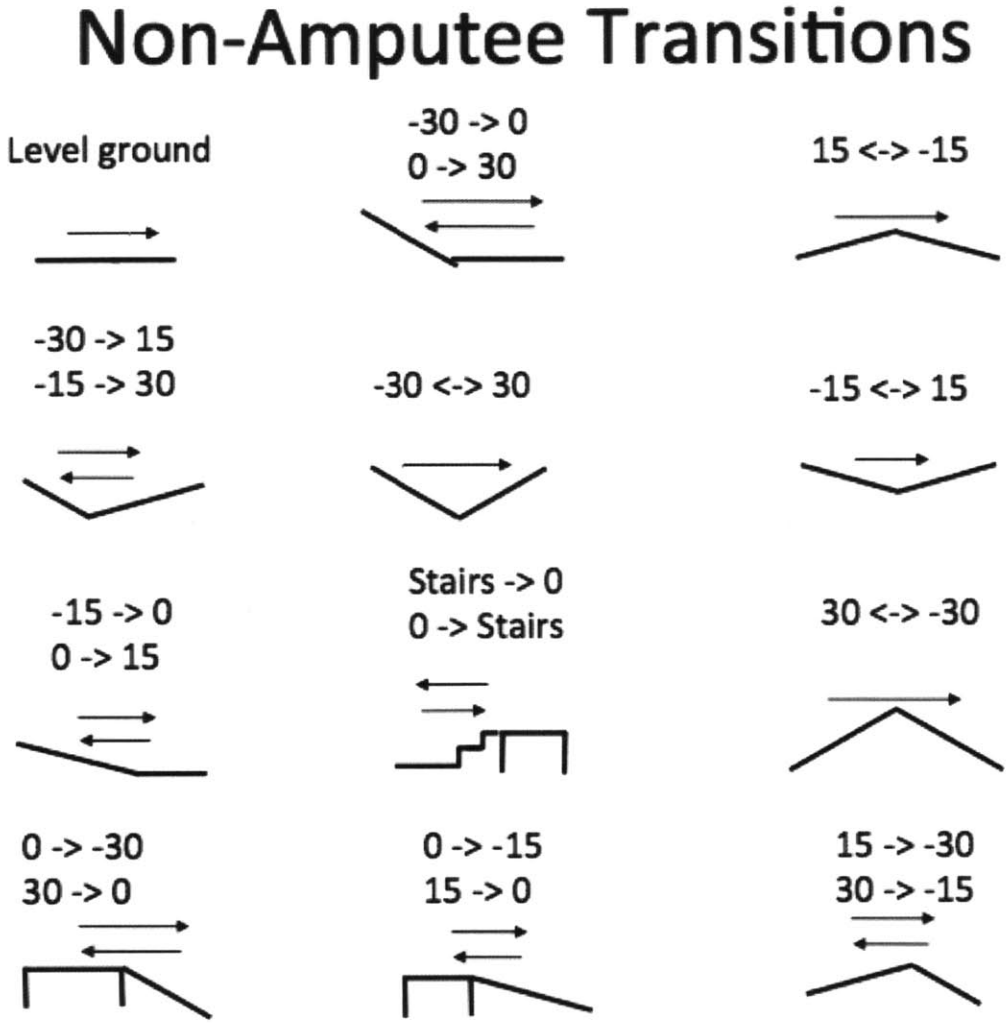

Figure 4-2: Arrows indicate the first direction of travel and then going back in the opposite direction. If up and down stairs are included this results in 19 total transitions. The transitions were physically built to be wooden platforms with hand-rails. The level ground condition did not use a ramp or a wooden structure unless it was attached to a down-ward slope, to ensure safety during the transition to level-ground.

4.2.1 Obtaining a classifier

We obtained a classifier for each subject that classifies each of the 19 different terrain by using the algorithm described in Chapter 3. The process is worked out in

		Nave Bayes	Support Vector Machine
S1ABBD	Num Features	6	9
S2ABBD	Num Features	4	9
S3ABBD	Num Features	4	8
S4ABBD	Num Features	4	8
S5ABBD	Num Features	4	9
S6ABBD	Num Features	4	9
S7ABBD	Num Features	3	5
	Avg Num Features	4.1	8.1

Figure 4-3: The algorithm running with a naive bayes classifier performs better than supper vector machine with a linear kernel.

mathematical detail in the Appendix. Here is it is worth noting that we used SFFS with a 5-fold cross validation and a naive bayes classifier with a decision function that chooses the class with the highest probability of being the correct terrain.

4.2.2 Comparison of support vector machines and naive bayes performance

The algorithm chosen in this thesis uses only a naive bayes classifier. Any other type of classifier that produces predictions on terrains could potentially also be used. One other important type of classifier that could be used is the support vector machine.

Typically, the support vector machine with a linear kernel (other kernel types also didn't show an improvement), was the best kernel to use, but still produces models with about twice as many features. For this reason we chose the naive bayes classifier as the suggested one to use with these data.

4.3 Results of Clinical Study 1

The results of running this algorithm on non-amputee data show that it is possible to discriminate between each of the 9 ramp conditions with each subject. The multi-classifier approach does work, though it is limited by the fact that it uses a more complicated model that could make it less generalizable on new data. There are boundary cases where applying this algorithm would not make sense, such as when the number of degrees between terrain is too small (see Amputee with BiOM study). Also, we use sequential floating forward search with a naive bayes classifier because it performs well on the data – it does not make sense to use a classifier that results in a worse reduction or decreased the explanatory ability of the data, unless the resulting classifier had properties that made the model easier to work with beyond having fewer parameters.

The areas for concern are the sensitivity of the phase-dependent algorithm with data from amputee subjects are

1. chanes in the size of the analysis window;

2. could this algorithm work both above and below knee amputees;

3. and when using ramps that have a small angle between pre and post foothold what is the performance.

4.3.1 Non-Amputee results from sensor selection algorithm

After running the sensor selection algorithm described in Chaper 3 on a data set containing both extrinsic and intrinsic features, we arrived a reduced feature set that also maximized accuracy on individual subjects. Typically most participants had classifiers with more intrinsic than extrinsic sensors. We also studied the comparative result of just using intrinsic sensors, and then using extrinsic sensors from a simulated transtibial amputee that uses data from non-amputees later in this chapter. Those results suggest that for a practical system just intrinsic sensors should be sufficient for controlling a robotic ankle prosthesis.

4.3.2 Confusion Matrix Results

After we have obtained the classifiers that give us the most accurate and minimal set of features necessary to classify walking data into one of the 19 different classes outlined previously. Figure 7-8 contains the confusion matrix for each subject in order from 1 to 5. Note that most of the elements are on the diagonal. This means that the classifier is picking the correct transition almost all the time. However, the figures also show that some classifiers do confuse some conditions. The rows correspond to the true class and the columns correspond to the predicted class. Therefore, anything that sits "off-axis" is a miss-classification. The goal of our classifier is to minimize missclassifications to prevent improper functioning of the robotic limb.

Subject 1 Table		**Subject 2 Table**	
Feature	Accuracy	Feature	Accuracy
max shank x pos	0.602	min knee x pos	0.441
max knee z pos	0.854	waveform right m gastroc	0.838
waveform right glute max	0.947	rms knee y pos	0.937
AR(3) shank y pos	.977	mav knee y pos	0.977
mav ankle z	0.99	zcs right glute max	0.99
Subject 3 Table		**Subject 4 Table**	
Feature	Accuracy	Feature	Accuracy
ssc right m gastroc	0.472	min knee z pos	0.644
max ankle x pos	0.78	mav knee y pos	0.933
max shank x	0.876	min right glute max	0.97
min left vastus lateralis	0.934	mav shank y pos	0.99
min left semitend	0.972		
AR(3) right vases lateralis	0.99		
Subject 5 Table		**Subject 6 Table**	
Feature	Accuracy	Feature	Accuracy
rms ankle x pos	0.546	max ankle y	0.893
max ankle z pos	0.838	min shank z	0.957
mean right adductor magnus	0.94	ssc knee x	0.96
mav knee x pos	0.99	max knee x	1.0
Subject 7 Table			
Feature	Accuracy		
min ankle z	0.819		
max ankle z pos	0.838		
mean right adductor magnus	0.94		
mav knee x pos	0.99		

Table 4.1: The features, along with their respective sensors, are listed in the table above. The dominant features are all taken from the vicon markers instead of extrinsic sensors like EMG. This suggests that a strategy that uses primarily intrinsic sensors would adequately predict the 19 different ramp conditions from the trial. This is indicated by the 99% accuracy associated with the top features.

Ultimately, the purpose of the confusion matrix is to give a way for prosthesis designers to evaluate the effectiveness of the classifier on comparisons between terrains and find areas of potential improvement for each subject. Improvements could take the form of new control methods or heuristics that try disambiguate the distinct classes.

4.3.3 Sensitivity Analysis of Phase-Depdendent Algorithm

The algorithm the was derived for the use with non-amputees made no prior assumptions about how sensitive the features, and the performance of the models, would be to window length. In particular, if the extraction windows are too small or if the data are too noisy the algorithm might not work. The first experiment was to successively reduce the length of the data extraction windows, moving closer to the pre-foothold and early into swing phase Figure 4-6.

If the algorithm is sensitive to the amount of data in the windows then the reduction in the size of the window should result in a comparable change in the feature/sensor combination selected by the algorithm.

Table 4-6 shows the results of taking smaller windows on the types of features that come out of the algorithm. For almost all of the subjects (except maybe S3ABBD) the features derived by the algorithm are very stable. This suggests that to create a robust control system, that would work under potential time-dilations, is possible. The way to evaluate the table is by looking at each subject. Then within that subject see which features are changing. In all cases many of the features that are present at 25% of the window are also present at 50% of the window. Further, at 25% of the window, we were able to classify with 100% accuracy, so despite slight variation in the features the algorithm still produces reliable results at varying window sizes.

The results in Figure 4-6 can be interpreted using Figure 4-4. The "feature order" in

Sensor	Muscle	Ranges		Feature Order	
knee x	NA	1 to 11		1	autoregressive coef 1
knee y		12 to 22		2	autoregressive coef 2
knee z		23 to 33		3	autoregressive coef 3
ankle x	NA	34 to 44		4	rms
ankle y		45 to 55		5	mav
ankle z		56 to 66		6	zcs
shank x	NA	67 to 77		7	ssc
shank y		78 to 88		8	waveform
shank z		89 to 99		9	max
EMG		100 to 274		10	min
				11	mean

Figure 4-4: Glossary of feature numbers for non-amputee subjects.

		Full Window	**50% of Window**	**25% of Window**
Subject Name	**S1**	75, 31, 253	75,31,7	75,31,7
	S2	4,65,228	4,65,228	4,65,228
	S3	65,42,8	31,75,207	65,37,75
	S4	64,15,141	65,15,176	98,15,261
	S5	42,31,64	42,31,64	42,31,64
	S6	53,31,36	53,42,12	53,44,12
	S7	31,20,7	31,20,7	31,20,7

Figure 4-5: Results from running the sensor selection algorithm with reduced available decision sizes.

the figure indicates that ordered sequence the features were taken in. For example, feature 36 is actually autoregressive coefficient 3 of the knee z position.

Above and Below Knee Amputation Simulation

It is unclear, from the data, if the algorithm will work well on both above and below knee amputees. Upon removing the EMG sensors below the knee the algorithm should still produce results that suggest an IMU strategy is superior to one with EMG alone.

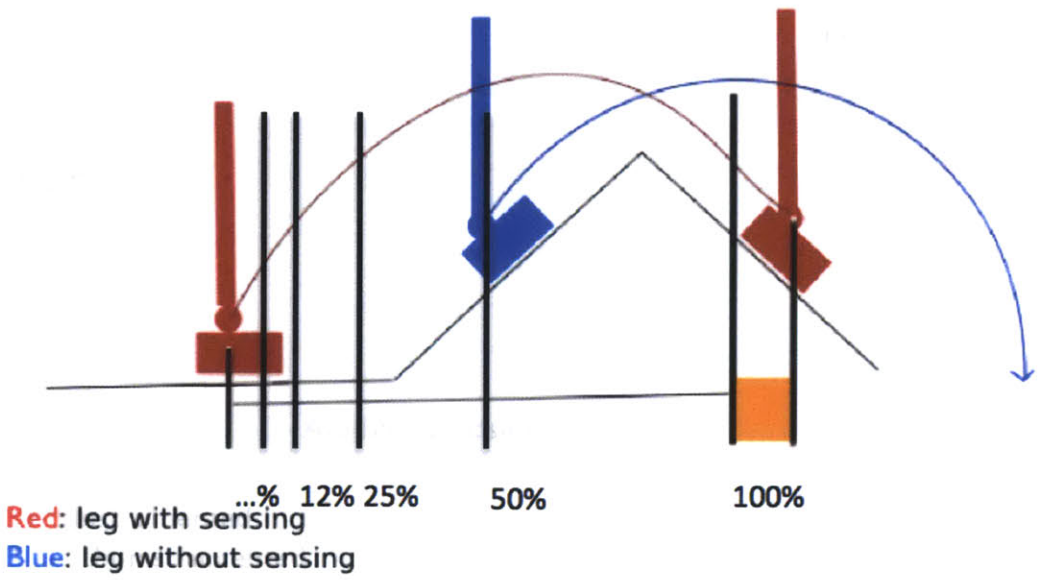

Figure 4-6: By reducing the size of the window by successive halves you reduce the amount of data available to algorithm. This tests the robustness of the algorithm.

The methodology in this analysis was to only use those data that corresponded to IMUs at the knee, shank, and ankle. When EMG was included we used the data from the residual limbs of a transtibial amputee in the below-knee case. Then we fused the IMU and EMG in one particular case at the feature level.

Indeed this is what we find in Figure 4-7 and Figure 4-8. The Above Knee EMG are, on average, about three times greater than using the EMG features from the IMU alone. While the EMG from the residual muscles in the simulated below-knee amputees require two times as many features as the case where IMU features alone are used.

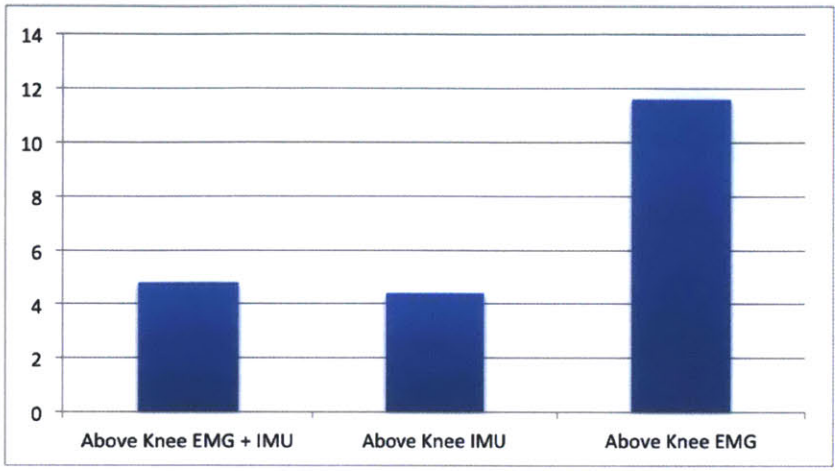

Figure 4-7: Using only EMG to control a prostheses through various terrain transitions is nearly three times as hard as just using features from IMUs.

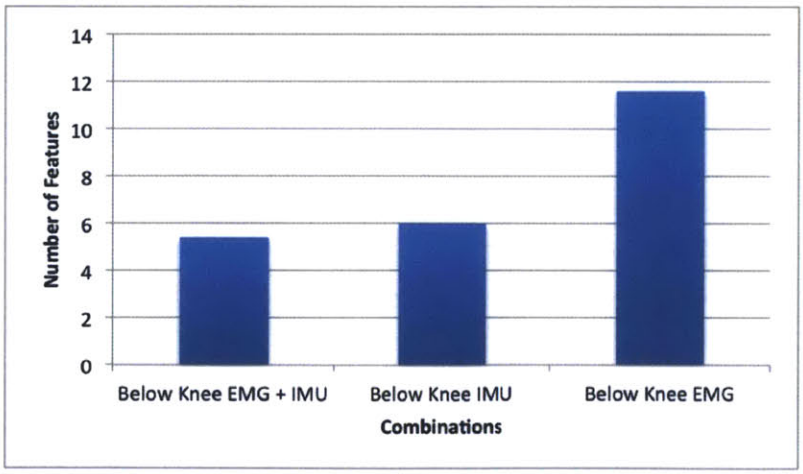

Figure 4-8: Using only EMG to control a prostheses through various terrain transitions is nearly two times as hard as just using features from IMUs.

4.3.4 Multiuser Classification

While the main algorithm of this thesis works well on individuals, one might want to build a more general classifier to evaluate the set of features that are most useful in classifying terrains for all participants.

One approach is to simply concatenate all the data together from all subjects after normalizing subjects and then run the same algorithm again. This was particularly effective with amputee subjects wearing the BiOm. Using an IMU that was reset after every heel-strike produce a common origin and frame among different subjects.

Mathematically, given a subject S there is an associated training data set $\mathbf{X}_S$ for each subject. The main algorithm, denoted $f : \mathbf{X}_S \mapsto f$, maps $\mathbf{X}_S$ to a function that takes new examples as an argument. Then for each subject there exists a classifier f^S for each subject, i. Then I propose that instead of having individual participant specific classifiers, we have one multi classifier that is trained from a stacked training matrix as follow.

Let $\mathbf{X}_{S_1}, \mathbf{X}_{S_2}, \ldots, \mathbf{X}_{S_n}$ be the training matrices for n subjects. Then let the total training matrix is denoted, $\mathbf{X}_{total} = \mathbf{X}_{S_1}||\mathbf{X}_{S_2}||\ldots||\mathbf{X}_{S_n}$, so that we obtain a more general classifier by applying this matrix as, $f(\mathbf{X}_{total}) = f_{multiclassifier}$.

Accuracy	Feature Number
Subject 1	
0.812 —	21
0.913 —	4
0.957 —	9
0.992 —	132
Subject 2	
0.859 —	9
0.986 —	26
Subject 3	
0.789 —	20
1.000 —	32

Figure 4-9: Using vicon markers gave a very sparse representation of the model's feature space. It also surprising to note that only one of the features selected belong to an EMG sensor. All of the others came from vicon markers.

4.3.5 Multiuser Classifier for Amputees wearing a conventional prosthesis

For each subject that was tested using the conventional prosthesis, we stacked those training data together and matched labels. The result is that the number of features does not increase dramatically, see Figure (insert figure). This was done using a combination of intrinsic and extrinsic sensors. Then the best sensors selected are those that work for all subjects and are more general.

Normalization with Z-Score only

We used two ways to normalize between subjects. The first is to normalize using the z-score and the other is to do so using a combination of biomechanical normalization combined with a z-score.

The data collected from subjects can be treated as a collection of random variables, $X \approx N(EX, \sigma(X)^2)$, drawn independently from a normal distribution. Then the z-score is defined mathematically as,

$$Z = \frac{X - E(X)}{\sigma(X)^2},$$

where $E(X)$ is defined as the expected value of the random variable X under the normal distribution. Assuming there is no bias in the expectation this is usually the sample mean taken from experimental data while, σ is the variance of the sample and is mathematically,

$$E(X - E(X))^2.$$

Often it is useful to look at this formula in terms of the individual samples taken from clinical data. Then the sample mean is $E(X) = \bar{X} = \frac{1}{n}\sum_{i=1}^{n} X_i$, where each exemplar is X_i for $i = 1 \ldots, n$ is taken from the rows of the dataset.

4.3.6 Best Set of Sensors and Features

Through all of these clinical studies the results consistently suggest across amputees and non-amputees that intrinsic sensors only, are needed predict terrain transitions.

Obviously, we would like to implement these algorithms in a real robotic ankle to predict terrains.

The study in Chapter 5 uses transtibial amputees and real IMU data collected from the ankle, that is the same as the data that would be collected while an amputee would be walking on the experimental transitions. These data suggest that the IMU coming from the ankle and the constituent estimates about height and distance would be enough to predict all 9 terrain the amputees were asked to walk over. Between those ramp conditions a controller that utilized the passive compliance of the ankle would be enough to adapt to the terrain difference between pre-foothold and post-foothold.

4.4 Conclusions

The results suggest that an intrinsic control strategy could be used for terrain adaptation on 19 different ramp transitions. The non-amputee study covered in this chapter, that was run with vicon markers with non-amputee extrinsic data suggest that the simplest model that is most likely to generalize is one that uses intrinsic data taken from an IMU and has been processed to have similar accuracy as the vicon markers. Extrinsic sensors, such as EMG, have problems with donning and doffing that would make their application to a robotic prosthesis worn daily difficult.

Chapter 5

Clinical Study 2 - Amputee with Powered Ankle Prosthesis

5.1 Participants

In order to test the performance of this algorithm on a real robotic prosthesis we collected data on seven transtibial amputee subjects while wearing a BiOM robotic ankle. We looked at IMU performance to see if there existed a strategy that resulted in very high accuracy on all 9 terrains with a single IMU. We show that, based on this experiment it was possible to achieve high levels of predictive accuracy with information that is only from the saggital plane of the IMU.

Each subject had EMG electrodes placed on their vastus laterals, gluteus maximus,

Subject ID	Age	Weight (lbs)	Height
Subject 1	33	192	5' 10"
Subject 2	38	150	5' 8"
Subject 3	38	200	6' 3"
Subject 4	31	185	5' 8"
Subject 5	26	165	5' 9"
Subject 6	46	195	5' 7"
Subject 7	47	160	6' 1"

Figure 5-1: The seven transtibial participants were age, weight, height matched.

rectus femurs, bicep femoris, adductor magnus, and their vastus medials. Markers were placed on the lower half of the body according to the Helen Hayes model. For these sets of experiments, the BiOM robotic ankle calibration was performed for each subject to make sure the actuation of the ankle was within biological constraints for the weight of the subject and comfortable for their use.

5.2 Methods

The calibration normalized how power should be produced during fast and slow walking. After this calibration phase each subject was asked to walk over a set of 9 terrain transitions, Table 5-2. An additional experiment was run with ramps ranging from 2 to 6 degrees to measure resolution of the main algorithm when applied to IMU position data.

The algorithm described in Chapter 3 was applied here using windows that were 0.4 seconds long. Then the training matrix was applied with only IMU data using SFFS,

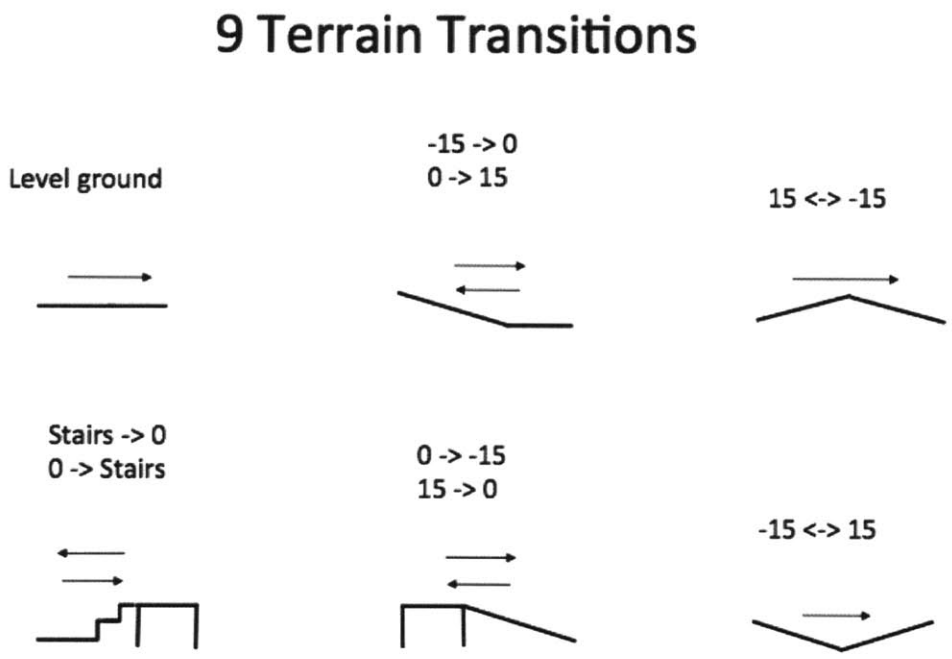

Figure 5-2: During this experiment 9 ramp transitions were used to simulate an environment with varying terrain.

and a 5-fold cross validation with a naive bayes classifier. The features extracted were consistent with those described in Table 7-1.

The IMU data were taken from the BiOM ankle and vicon marker data, were taken from motion capture, are very similar both qualitatively and quantitatively. To give the reader a more qualitative description of the accuracy, here we show one particular transition that is often important is going from a downhill ramp to level-ground. In Figure 5-3 and Figure 5.2, the two curves are similar and the average distance between the two curves (taken point-wise), was about 3.08 cm in height by the end and 12.5 cm in distance over the course of approximately 0.6 seconds (60 samples * 1 second

/ 100 samples).

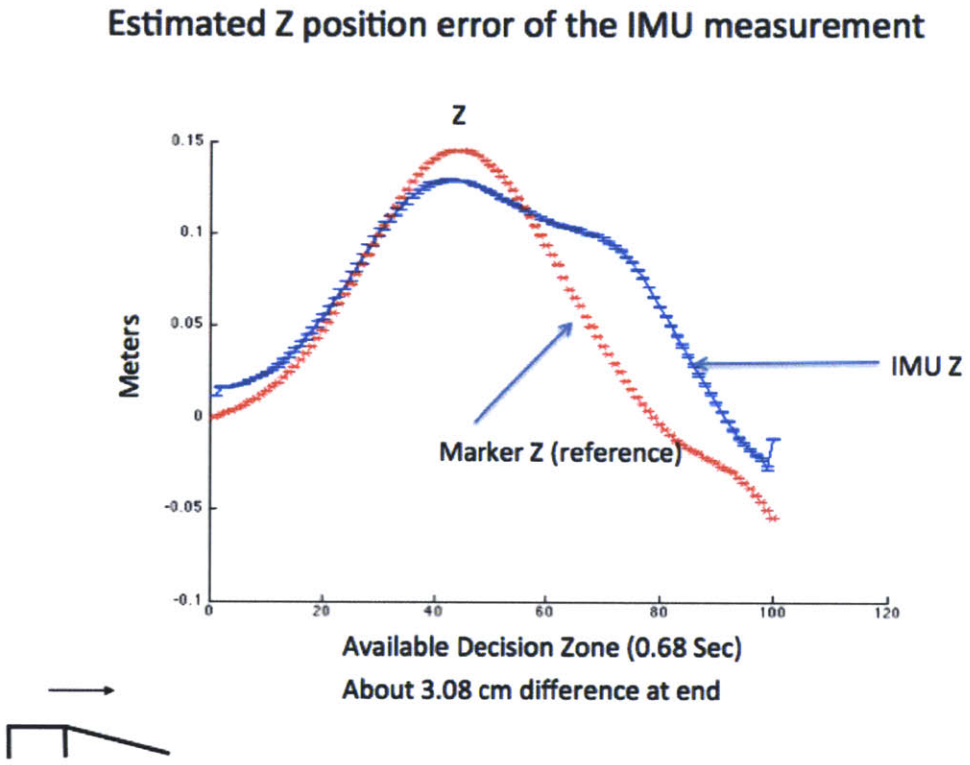

Figure 5-3: The trajectories of the IMU and the Markers are very similar both in maximum height and minimum height. The final distance between both curves was 3.08 cm

The typical decision window length was around 0.6 seconds long. Then the 0.3 second sliding windows were used to extract features from the available decision zone as depicted in Figure 5-5. This resulted in a about 30 examples by 11 features per signal times the number of signals for a particular participant. As an example, a the structure of a typical training matrix is depicted in Figure 5-6.

These training matrices were then analyzed using the algorithm described in Chapter 3 with a naive bayes classifier and the sensors and features described above.

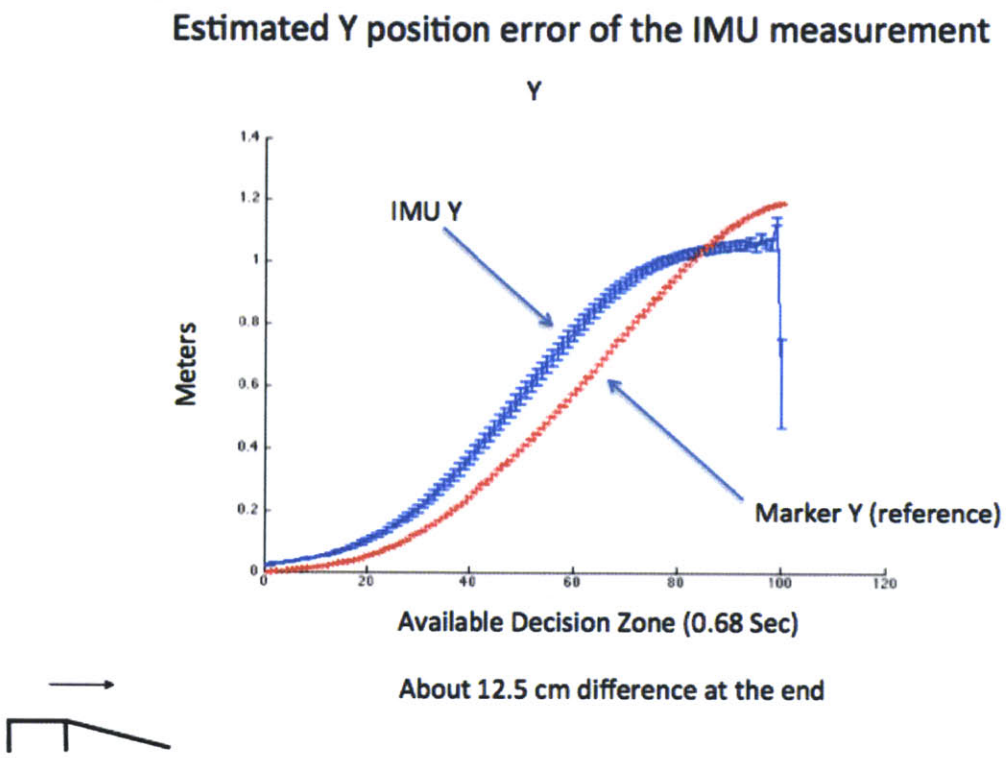

Figure 5-4: The trajectories of the ankle in forward motion as measure from the ankle by an IMU (blue
and vicon marker data (red). As in the previous case the difference between the two curves is small and they qualitatively look appropriate. The distance between curves is about 12.5 cm.

5.3 Results

Overall, with seven transtibial amputee subjects, and real IMU data the algorithm was able to find a strategy using only sagittal plane directions. In Figures 7-13, 7-14, 7-15, 7-16, 7-17, 7-18, 7-19 the reduction was still significant with a naive bayes classifier that performs with at least 95% accuracy (from the original feature space since the reduction went from 192 features to an average of 14 features (a 92% reduction)). The features had overlap between subjects. However, many of the features are slightly

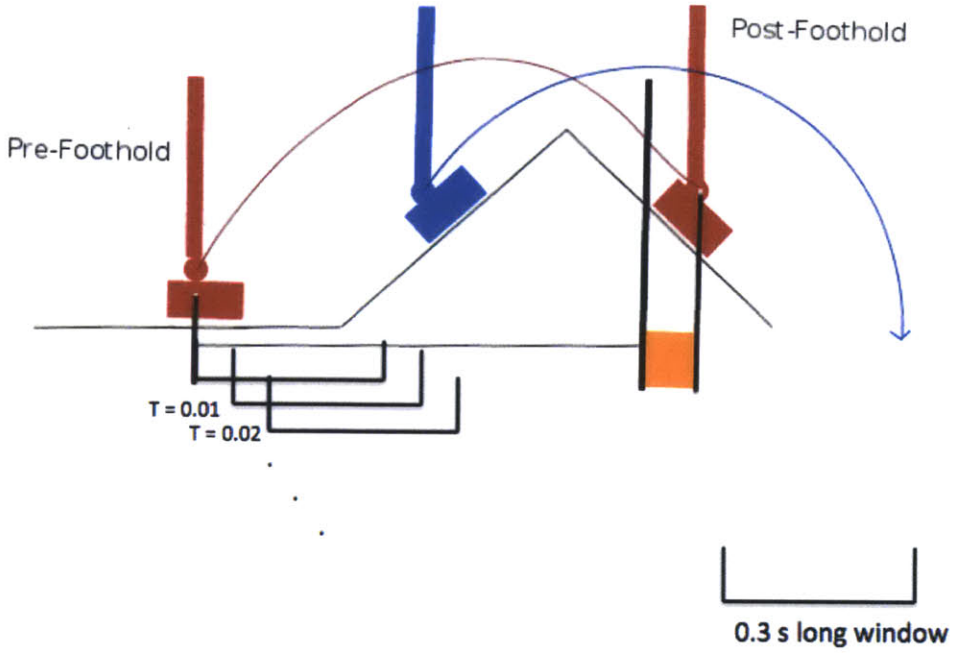

Figure 5-5: To build the training matrix we extracted data from a sliding window, applying 11 features to each signal. From that approximately 30 rows in the training matrix were produced.

	Feature 1	Feature 2	Feature 3	Feature 4	Feature 5	Feature 6	Feature 7	Feature 8	Feature 9	Terrain Number
Time 0.01	-0.997	-9.99E-05	0.0207	2.1976	2.1792	0	0	0.0504	2.4693	1
Time 0.02	-0.997	-3.94E-05	0.0207	2.2178	2.2013	0	0	0.0504	2.471	1
Time 0.03	-0.998	5.72E-06	0.0208	2.2373	2.2224	0	0	0.0507	2.4721	1
Time 0.04	-0.998	-0.0002	0.0209	2.2559	2.2427	0	0	0.0505	2.473	1
Time 0.05	-0.998	-9.83E-05	0.0208	2.2738	2.2621	0	0	0.0503	2.4736	1
Time 0.06	-0.997	-0.0002	0.0208	2.2908	2.2805	0	0	0.0503	2.4746	1
Time 0.07	-0.997	-0.0001	0.0206	2.307	2.2981	0	0	0.0504	2.4754	1
Time 0.08	-0.997	-0.0001	0.0205	2.3224	2.3147	0	0	0.0502	2.4762	1
Time 0.09	-0.997	-3.15E-05	0.0204	2.3369	2.3303	0	0	0.0503	2.4768	1
Time 0.10	-0.992	0.00037	0.0172	2.7158	2.689	0	0	0.0304	3.2318	2
Time 0.11	-0.991	0.00029	0.0167	2.6852	2.6571	0	0	0.0289	3.2187	2
Time 0.12	-0.991	0.00035	0.0162	2.654	2.6247	0	0	0.0279	3.2031	2
Time 0.13	-0.99	0.00024	0.0157	2.6223	2.5919	0	0	0.0269	3.1854	2
Time 0.14	-0.989	8.32E-05	0.0154	2.5902	2.5587	0	0	0.0267	3.1655	2
Time 0.15	-0.989	-7.12E-05	0.0151	2.5577	2.5252	0	0	0.0271	3.1436	2
Time 0.16	-0.988	-0.0002	0.0149	2.525	2.4916	0	0	0.0283	3.1205	2
Time 0.17	-0.988	-0.0001	0.0145	2.4922	2.458	0	0	0.0306	3.0966	2

Figure 5-6: The rows of a training matrix are extracted from the analysis windows and the columns are the features extracted during the sliding window procedure.

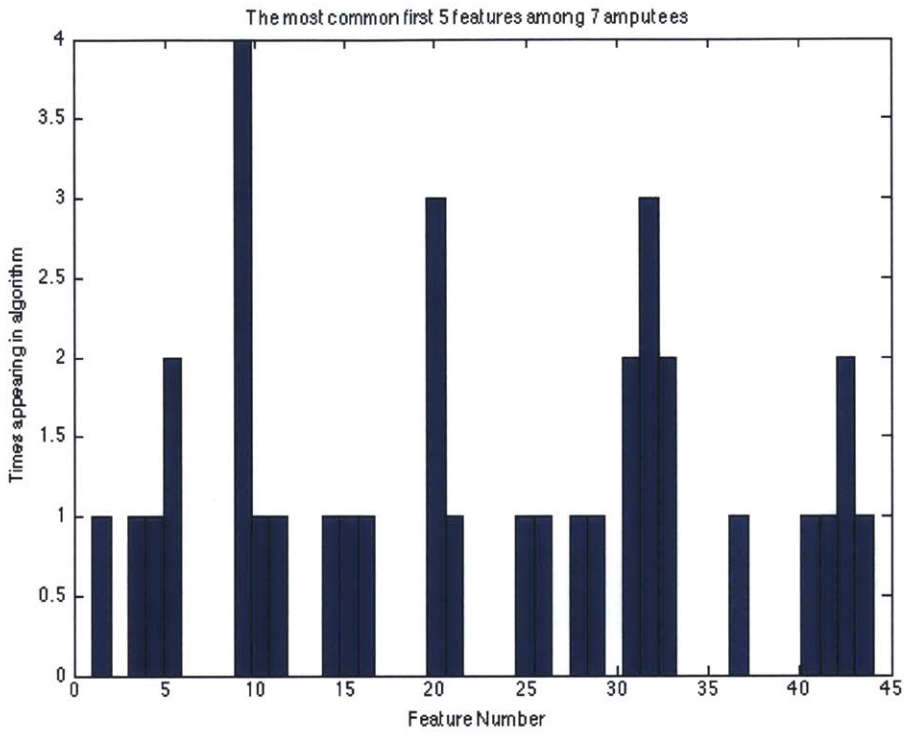

Figure 5-7: This figure shows the most frequently powerful features. Found by taking the first five features and then seeing which one are the most common. The most frequently powerful is the maximum of the ankle y position. Among the features that do appear (many do not appear at all), 28% of the features appear twice, 7% appear, 65% appear once.

different between participants. Figure 5-7 shows all of the features among the 7 different amputees collected and plotted to show frequency. These data suggest that predicting all terrain with just an IMU is possible, suggesting our hypothesis.

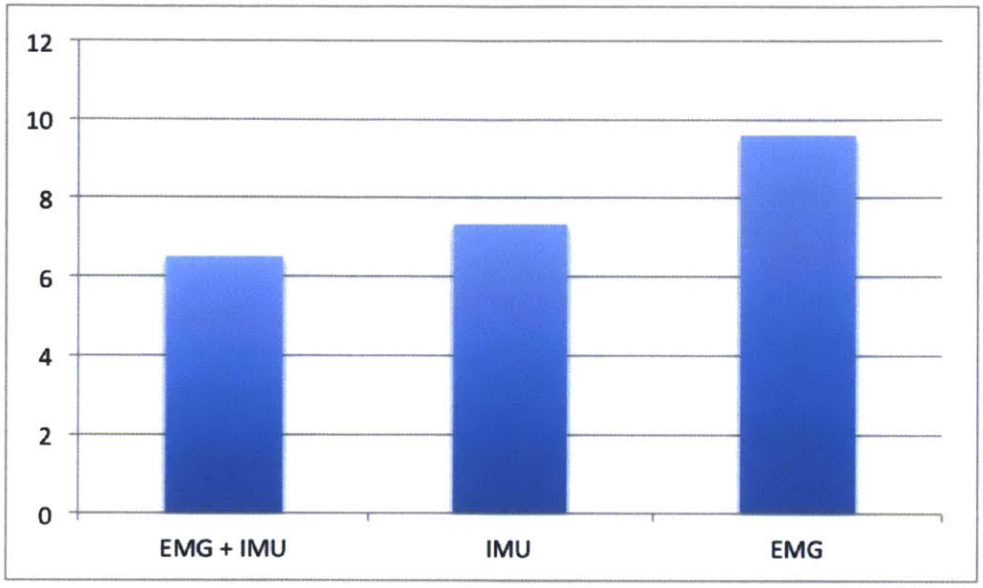

Figure 5-8: Similar to the non-amputee case the amputee with a BiOm also had that the IMU alone is simplest model and most practical model to use.

5.3.1 Comparison of EMG and IMU sensing with Robotic Prosthesis

In the previous study with non-amputees, we wanted to understand the trade off between extrinsic and intrinsic sensing as sensing methodologies. In this part of this study we compared the results if we used only intrinsic sensing, here IMU, and compared it to extrinsic alone, and combining both to see which model was simpler. By averaging the results over all 7 subjects we can see that the model with the smallest number of parameters is the one created with IMU and EMG. However, donning and doffing problems associated with EMG make it less desirable than just using the IMU model, that has only a few more features in it's model, Figure 5-8.

Source Glossary	
Ankle Y	1 to 11
Ankle Z	12 to 22
Knee Y	23 to 33
Knee Z	34 to 44
Feature Glossary	
1	autoregressive coef 1
2	autoregressive coef 2
3	autoregressive coef 3
4	rms
5	mav
6	zcs
7	ssc
8	waveform
9	max
10	min
11	mean

5.3.2 Multiclass Considerations

There are two primary ways to process each subject's data:

1. Concatenate all the subject data into one large training data set and then process

2. Train each subject individually generating user specific classifiers

The primary trade-off between 1) and 2) is that by combining all the data together there are more features that results from the main algorithm. By using a subject specific classifier the solution has fewer features, in comparison to the case where a classifier is trained for all subjects.

In Table 5-9, the results suggest that it is possible to combine all of the training data together and use the same algorithm that was developed for individuals and apply it across subjects. However, this is at the cost of having a simpler model, that is, fewer features. The trade-off is actually is actually quite drastic, see Table 7-13, Table 7-14, Table 7-15.

Among the features that do appear twice or three times the following patterns can be discerned.

- 3 x root-mean-square, 3 x mean-absolute-value, 2 x mean were the transformations that appeared the most frequently among mapping of the sensors;
- Each of the sensors are fairly well represented.

If myographic signals were going to be very powerful, as a source to use for discrimination with the BiOm, then it should have produced a powerful classifier and EMG features separate classes on-par or faster than features taken from intrinsic sources. As it stands the performance of surface EMG was unable to match using real IMU data obtained on the BiOm.

5.3.3 Small ramp analysis

Another confounding condition to be aware of is the limits of discrimination among users of a controller that adopts this methodology. When the difference between

Feat Num	Classification Accuracy	Feature Type	Feature Type	Source		
1 —	0.358 —	20	max	Knee Y		
2 —	0.484 —	11	mean	Ankle Z		
3 —	0.507 —	17	waveform	Knee Z		
4 —	0.540 —	33	mean	Knee Y		
5 —	0.559 —	9	max	Knee Y		
6 —	0.606 —	37	rms	Ankle Z		
7 —	0.629 —	10	min	Ankle Y		
8 —	0.663 —	22	mean	Knee Z		
9 —	0.684 —	1	autoregressive coef 1	Ankle Y		
10 —	0.702 —	8	waveform	Ankle Y		
11 —	0.724 —	30	waveform	Knee Y		
12 —	0.745 —	29	ssc	Ankle Y		
13 —	0.758 —	18	ssc	Ankle Z		
14 —	0.779 —	31	max	Knee Y		
15 —	0.786 —	21	min	Ankle Z		
16 —	0.807 —	28	mav	Knee Y		
17 —	0.810 —	2	autoregressive coef 2	Ankle Y		
18 —	0.827 —	3	autoregressive coef 3	Ankle Y		
19 —	0.830 —	7	ssc	Ankle Y		
20 —	0.852 —	42	max	Knee Z		
21 —	0.846 —	6	zcs	Ankle Y		
22 —	0.857 —	43	min	Knee Z		
23 —	0.854 —	23	autoregressive coef 1	Knee Y		
24 —	0.856 —	19	waveform	Ankle Z		
25 —	0.865 —	32	min	Knee Y		
26 —	0.874 —	38	mav	Knee Z		
27 —	0.874 —	12	autogressive coef 1	Ankle Z		
28 —	0.877 —	41	waveform	Knee Z		
29 —	0.875 —	4	rms	Ankle Y		
30 —	0.874 —	13	autoregressive coef 2	Ankle Z		
31 —	0.871 —	14	autoregressive coef 3	Ankle Z		
32 —	0.878 —	25	autoregressive coef 3	Knee Y		
33 —	0.882 —	26	rms	Knee Y		
34 —	0.892 —	24	autoregressive coef 2	Knee Y		
35 —	0.902 —	40	waveform	Knee Z		
36 —	0.886 —	5	mav	Ankle Y		
37 —	0.892 —	15	rms	Ankle Z		
38 —	0.900 —	16	mav	Ankle Z		

Figure 5-9: This table shows the result after combining three amputee subjects together. Then we run the main algorithm to get one model to predict nine different terrain. The sources of data were limited to the Ankle Y/Z position and the Knee Y/Z position – essentially sagittal plane motion.

Maximal Accuracy Achieved Before 0.95 accuracy				
	Subject 1	Subject 2	Subject 3	Subject 4
2 degree difference	0.75	0.95	0.85	0.95
4 degree difference	0.95	0.95	0.93	0.95

Figure 5-10: These results suggest that trying to classify at small ramp angle is difficult and many not produce a useful classifier below a 4 degree difference in terrain.

ramp conditions becomes tiny the main algorithm should have difficult in telling the difference between the slopes of the terrain.

The feature space shown in Figure 5-15 shows the space when then world consists of level ground, $\pm$ 15 degree ramps, and $\pm$ 8 degree ramps. The distance between clusters of points is important in establishing the discriminability of two classes.

To further, analyze this situation we conducted a smaller study with four amputees walking,

- level ground to positive 2 degrees and 2 degrees down to level ground
- level ground to positive 4 degrees and 4 degrees down to level ground

The results of running this algorithm with 0.2 second window lengths inside the available decision zone result mixed results for 2 degrees and acceptable results for 4 degrees 5-10.

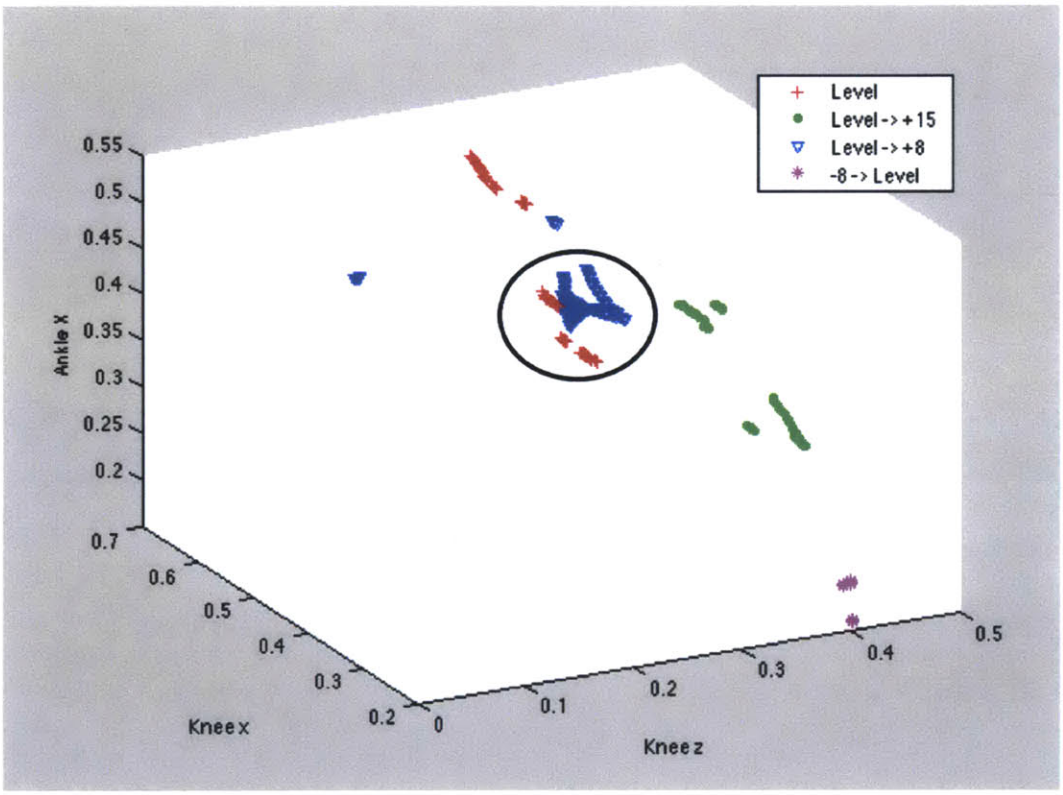

Figure 5-11: In the case of an amputee walking on ramps with a smaller degree difference, discriminability becomes slightly more difficult. Note that the Level (red) and Level to +8 condition are similar.

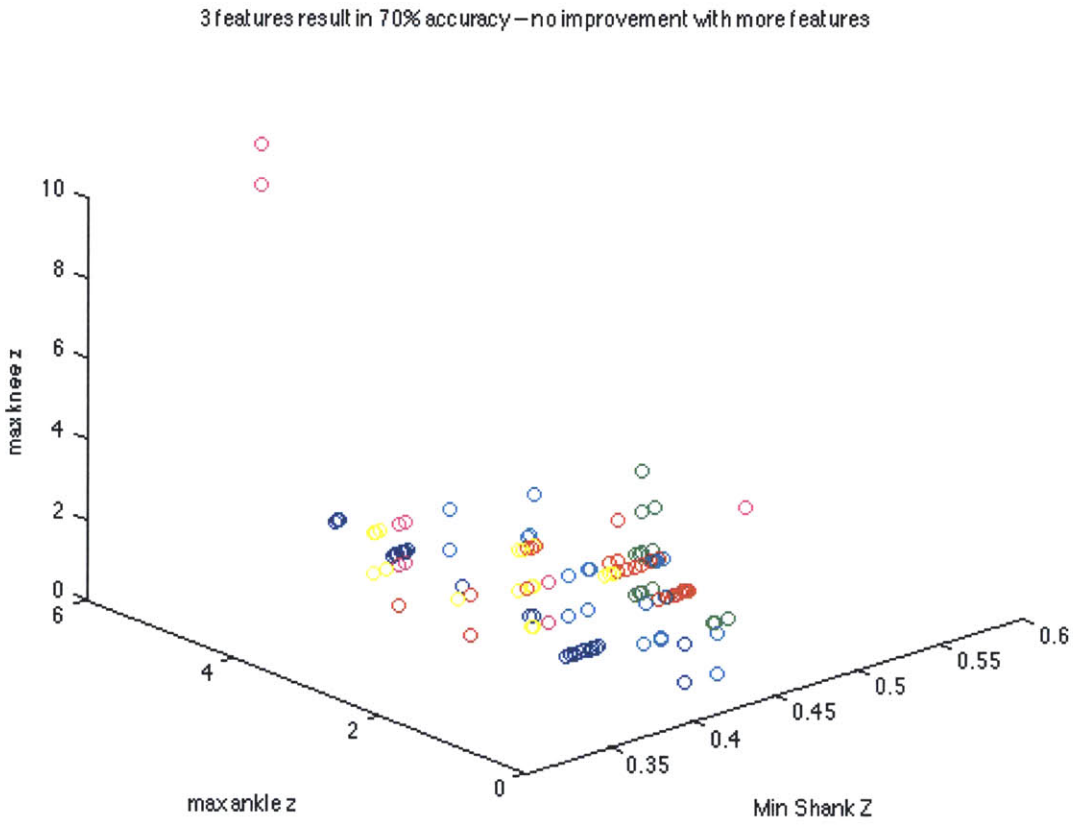

Figure 5-12: The feature space for this subject is very cluttered and scattered. The motions for small degree ramps are too similar to effectively discriminate between conditions.

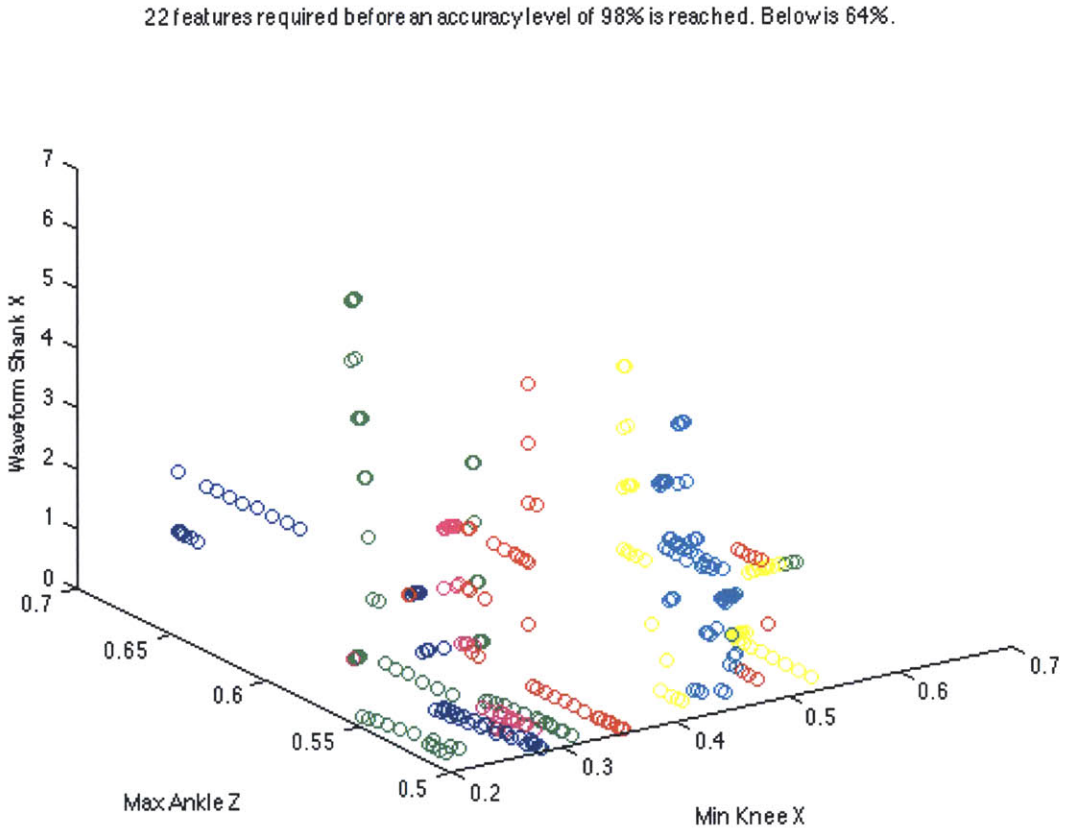

Figure 5-13: Again the feature space for this subject is very cluttered without clear divisions between small angle classes. However, a model was found with 22 features, but relative to the reductions apparent in other cases this is a very complicated model.

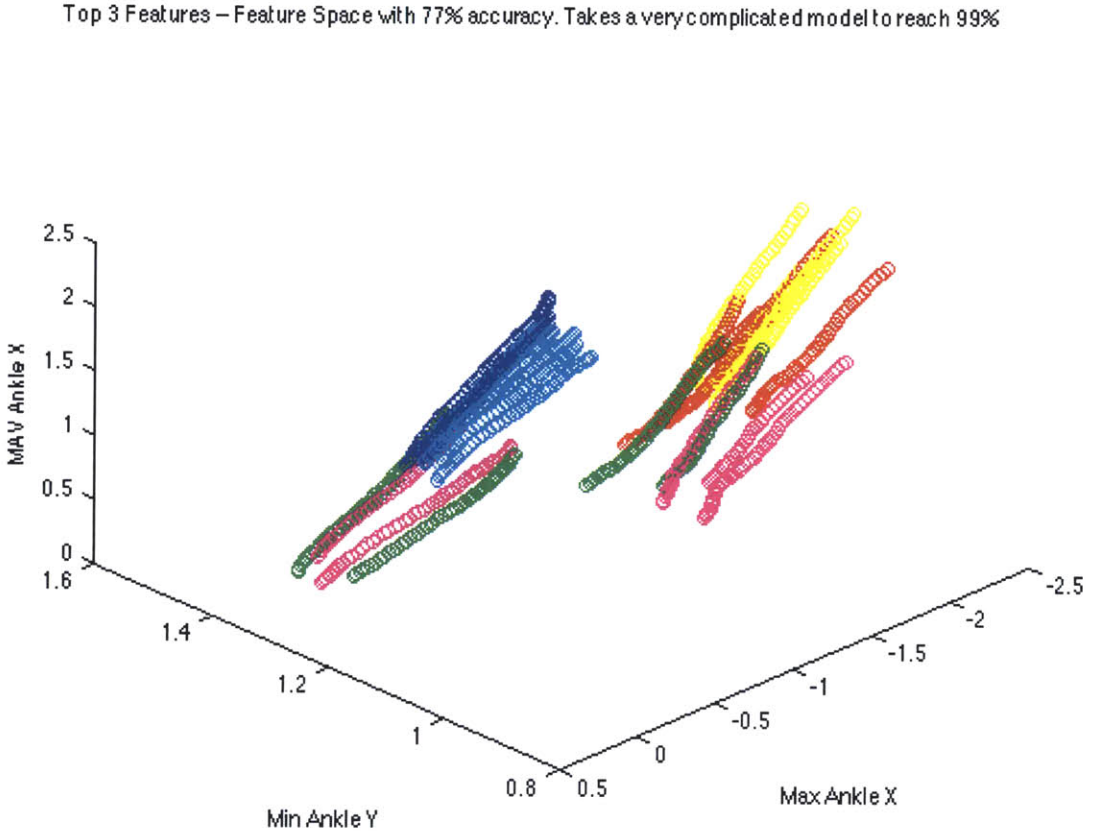

Figure 5-14: Again the feature space for this subject is very cluttered without clear divisions between small angle classes. However, a model was found with 16 features to get 99%, but relative to the reductions apparent in other cases this is a very complicated model.

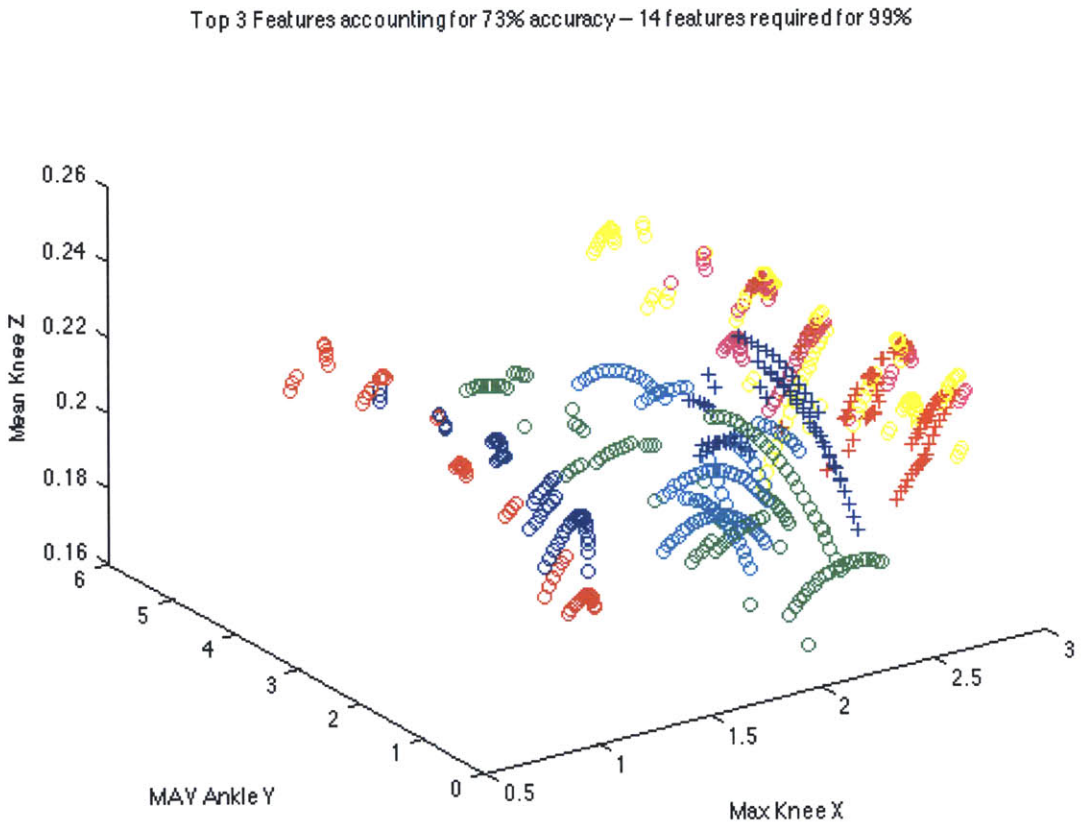

Figure 5-15: Again the feature space for this subject is very cluttered without clear divisions between small angle classes. However, a model was found with 15 features to get 99%, but relative to the reductions apparent in other cases this is a very complicated model.

5.3.4 Analysis of the relationship between slope degree and discriminability

The proposed algorithm in this dissertation should be accurate for a range of ramps between flat ground and 15 degrees. To test this, we conducted studies with 8 degree ramps to simulate the discriminability of ramps that amputees would encounter in a real-world situation.

To test this we conducted a study with four amputees wearing a BiOm prosthesis. The intrinsic sensing was a simulated IMU that took data from the ankle and knee. EMG was left out, because we have established for 15 degrees differences that with data from a single IMU, that has been integrated so that we have positions, and translated to the position of the ankle and the knee, that the IMU at the knee and ankle, can perform robustly for larger degree changes.

The results are interesting, because the algorithm is able to work on these small ramp transitions as well. However, the feature reduction in all cases was far less than the case of more drastic transitions. In comparison, for non-amputees the reduction was very significant for all terrain types with a vicon marker with far more terrain. In comparison, this is not as strong a reduction with a threshold of 95% accuracy and suggests that the algorithm is having difficulty with such small variations in terrain, Figure 5-16.

The use of the algorithm appears to be limited to degree transitions that are greater

than or equal to 4 degrees. A further study should be conducted to exhaustively test all degree transitions between 0 and 15 degrees to parameterize the exact level of accuracy one can expect in an actual device.

Classification Accuracy	Feature Number
0.347 —	31
0.511 —	4
0.579 —	21
0.649 —	15
0.677 —	1
0.715 —	8
0.748 —	18
0.778 —	27
0.790 —	25
0.815 —	10
0.842 —	12
0.851 —	29
0.853 —	11
0.867 —	20
0.886 —	22
0.906 —	19
0.914 —	32
0.917 —	30
0.925 —	26
0.923 —	9
0.930 —	23

Figure 5-16: Despite there existing a relatively powerful classifier to determine the difference between level ground, 2,4,and 6, degree ramps the simulated IMU is more accurate than an actual IMU. Due to this the reduction witnessed here would be expected to be worse in that case and more difficult to classify.

Chapter 6

Clinical Study 3 - Amputee with Conventional Prosthesis Study

The main algorithm finds the minimal features and sensors that discriminate between each terrain condition with near perfect accuracy for non-amputees. The advantage of this algorithm is that it works generally across amputees and non-amputees wearing conventional prostheses. Below is a study conducted to confirm the proposed hypothesis that the EMG should be even weaker in an amputee's lower limbs, so the algorithm will find that IMUs are the preferred sensor over EMG.

6.1 Small Study Summary

Similar to the non-amputee study we have amputees walk over a given set of ramps and stairs, along with, level ground. Each amputee wore their self-chosen conventional prosthesis. Conventional, in this case, refers to there being no motorized or computer controlled actuation on the device beyond passive spring behavior. Some of the amputees used a prosthetic liner produced by Alps that has EMG leads stitched into the fabric to read signals from the medial gastrocnemius, lateral gastrocnemius, and the tibialis anterior muscles of the amputee, Figure 6-1. However, eventually this liner was abandoned in favor of a conventional liner. It turns out very few amputees had sockets that would fit the EMG liner. If we forced them to use it, their gait would have been affected due to a phenomena called, "pistoning".

Transtibial amputees will often have difficulty navigating steep slopes for long periods of time. In later studies the conventional prosthesis condition was replaced by a robotic ankle prosthesis (BiOm) that fires at inappropriate times during walking and as a result this study removes all conditions that contain a 30 degree ramp Figure 5-2.

The study was run on three unilateral amputees, and one of them used an 8 degree ramp in addition to the the full set. On each person a full set of EMG, IMUs, and markers were used. In general, there were fewer features required to perfectly discriminate the different terrain conditions in comparison to the non-amputee study.

This is likely due to the removal of the 30 degree condition. However, 30 degree ramps are rare in the typical urban environment, so the range of ramps used in the study are still realistic. Beyond that there is also the possibility that an amputee's gait, being slightly pathological with a conventional prosthesis, actually enhances the ability of pattern classifiers to detect terrain transitions.

The difference between level ground and 15 degree ramps is still rather large (for example see Figure 7-6), and some might argue, too large to pose a challenge to the prediction task – especially when most urban handicap ramps are approximately 8.5 degrees.

On 8.5 degree ramps the main algorithm is still able to differentiate between conditions with a minimal set of features, Figure 5-15. This is signifiant because in order for the classifier to work you have to produce a good enough signal to noise ratio, so that clusters are easy to discriminate. However, beyond this the BiOm ankle is able to handle variations in terrain that are less than this degree, so a specific control of the ankle might not be needed.

This study shows that it is possible to discriminate with 100% accuracy between the each ramp condition using only intrinsic sensing. For example, consider Figure 7-3, where the first feature, the maximum of the ankle height, was able to discriminate with 90% accuracy. Adding the second feature results in a classifier that discriminates among the 9 different terrains with 100% accuracy. The reason for this powerful

discrimination has to do with the different heights and lengths of swing associated with each terrain transition. For example, consider Figure 7-4, where only two features are needed for S1A to get to perfect discrimination. In this case the space was well separated into regions. One hypothesis, is that the geometry of the transition is fundamentally different once you consider the heights of the ramps and the length of the stride for each individual.

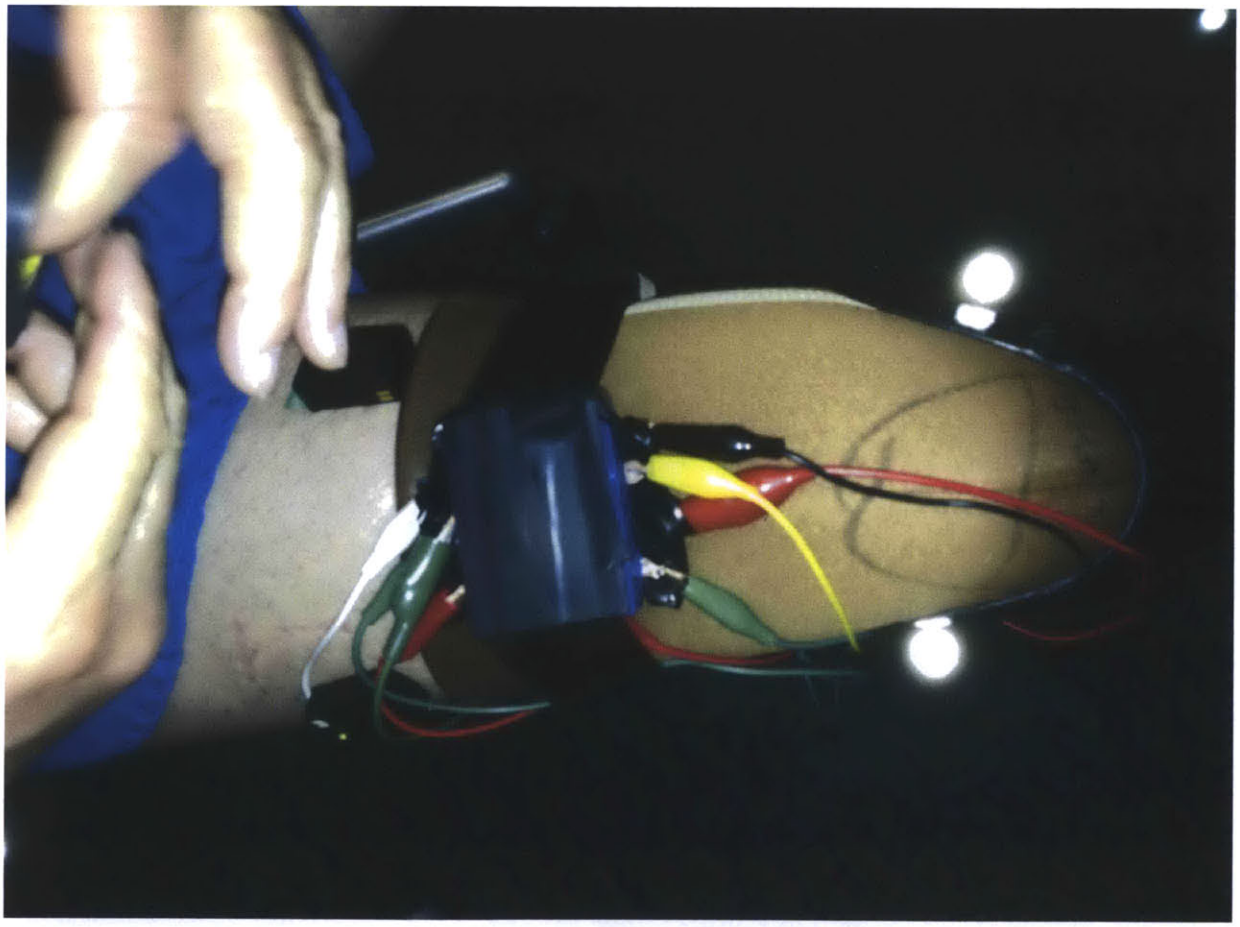

Figure 6-1: In order to record signals from inside of the socket, a typical Alps liner was modified with EMG leads placed inside the socket to record the signals from the residual Tibialis Anterior, Medial and Lateral, Gastrocnemius.

Chapter 7

Conclusions

7.1 Future Work

This work highlights how powerful the height and reach measured from one IMU can be determining terrain. IMU data is capturing the motion of our bodies, and our bodies in response to the ground beneath our feet. This interaction is reflected in the motion of limbs to avoid, to respond to, adjust, and slow our bodies down over varying terrain. However, despite all of these complicated motion a simple sensor can make each of these adjustments clearer.

This work opens up new directions for future reach in biomedical engineering and product design. By building on this work it is my hope to one day see amputees dancing and hiking with more ease than non-amputees.

7.1.1 Further Refinements

The algorithm presented in this thesis has been taken to the point of being ready for hardware implementation. Implementing this on hardware involves taking the presented classifier and building a digital controller that runs continuously, so that after heel-strike the classifier determines the current terrain right before post-foothold.

7.1.2 New Directions

This algorithm is quite general and the fact that it works with amputee gait also suggests it might be useful with predictions of other types of gait. One potential area of future work might be in identifying if children have autism based on their gait. Gait pathologies have been cited in cases involved children with developmental issues and this could be a warning sign that can be applied.

Another interesting connection to draw is the similarity of this method and hand writing recognition used on tables and PCs. The motion of the leg over terrain is similar to a finger tracing the outline of a letter. By drawing this connection the basic pattern recognition algorithm could be improved with as more data is collected.

7.2 Final Conclusions

The main contributions of this thesis are summarized as,

- Intrinsic sensory information is sufficient to detect a large number of terrain.
- The forward and vertical motion of the ankle and knee provide 95% accuracy on 9 terrain for amputees.
- The forward and vertical motion of the ankle and knee provide 95% accuracy on 10 different terrain for non-amputees
- Novel methodology in-terms of approach of using features to drive insights about sensors from a set of data.
- Largest amputee and non-amputee number of subjects compared to similar relevant literature (7 non-amputee and 7 amputee).
- Largest variety of transitions collected compared to similar relevant literature (19 for non-amputee and 9 for amputee).

The results of this thesis suggest the hypothesis that one IMU can differentiate with 95% accuracy between 9 different terrain conditions. To study this question we developed a hypothesis that looked at the role of EMG in non-amputees and amputees wearing a BiOM prosthesis. To determine the role of EMG we used a sequential floating forward feature selection algorithm with features common to EMG and IMU processing. Also we used an established sliding window technique to pick those sensors that contribute most to making a classifier robust.

In each case, IMU sensors were able to accurately determine the type of transition between pre and post foot hold. In the case of using actual IMU data from the BiOM, versus vicon data, the most relevant sources of data are those that deal with translations and the height of the foot moving through space.

As a result, designers of terrain adaptive robotic prostheses can use sagittal plane translations and heights to accurately predict the terrain prior to post-foothold. Based on the clinical studies contained in previous chapters this appears to be possible. The studies indicated that very few features are needed to predict a large range of terrain with a modest classifier.

In the case of a non-amputee the reduction using the main algorithm – the feature space was very large and the number of conditions to be predicted was also relatively large at 19 different transitions.

As a caveat, the reduction in the number of terrain transitions did improve the performance of the classifier for the amputee case. This suggests that scaling up to a larger number of terrains could potentially decrease the performance of this type of classifier. However, in most practical settings encountered in the real world, the set of transitions that were chosen is exhaustive and easily cover handicap ramps up, as well as, steep roads that would be encountered in many urban areas or while hiking.

Another potential area for future improvement would be to find ways to improve the detection of slight terrain variation below 4 degrees. At 4 degrees we observed from

four amputees that powerful discrimination could be obtained, but the results below 4 degrees were inconsistent.

This algorithm enables the development of controllers for robotic limbs to implement terrain adaptive controls. It helps a prosthesis designer choose which sensor modality will perform at a level that an amputee will require in daily tasks. It is also flexible enough for the addition of other sensors. The flexibility of the algorithm lies in linear dependency of sensors being used in this algorithm – adding one sensor just increases the size of the space that the search algorithm has to act over.

Appendix

Appendix A - EMG Feature Extraction

The features that are used throughout this work are derived from literature as those that are most useful for pattern recognition in myoelectric prothsetic sensing, see Figure 7-1.

Perhaps the most difficult feature to understand are the *autogregressive features.* The EMG in some cases can be modeled as a linear AR time series such that,

$$x(n) = -\sum_{k=1}^{p} a_k x(n-k) + u(n),$$

Where x(n) is the recorded signal at time n and $n \in$ Z, where $\{a_k, k = 1, 2, \ldots, p\}$ are autoregressive model coefficients, p is the order of the autoregressive model, and $u(n)$ is the residual white noise. The autoregressive model assumes that the present value of the time series $x(n)$ is linear dependent on the past values of the time series

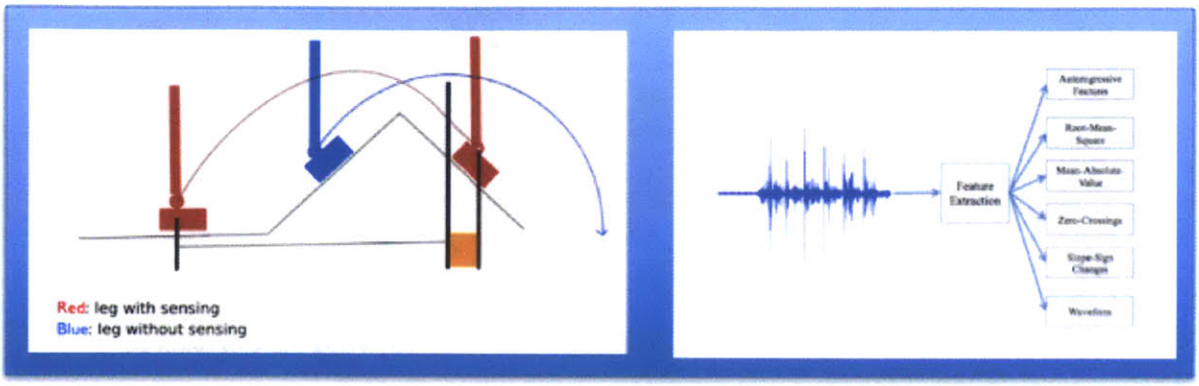

Feature Summary	
Feature Name	Description
Autoregressive	a 3×1 vector that contains the coefficients of a linear interpolation fit of
Root-Mean-Square	$\sqrt{\frac{1}{n}(x_1^2 + \ldots + x_n^2)}$
Mean-Absolute-Value	$\frac{1}{n}\sum_i^n \|x_i\|$
Zero-Crossings	Gives a rough idea of how the signal spectrum changes [27].
Slope-Sign Changes	The number of times the slope of the raw EMG signal changes.
Waveform	The length between adjacent samples, i.e. $\sum_i^n \|\Delta x_i\|$, where $\Delta x_i = x_i - x_{i-1}$
Min	the maximum value in the window
Mean	the mean value in the window
Max	the maximum value in the window

Figure 7-1: The features that are used in this thesis are a combination of features taken from literature on pattern recognition in electromyography and intrinsic sensing. They can both be applied to the either set of data.

$x(n-1), x(n-2), \ldots$ as described in [30].

Appendix B - Acquiring Positions from IMU Data

In the algorithm that is applied to the actual BiOm ankle, the position data of the ankle and knee is produced from a single IMU that is embedded in the ankle. The following work and insights are taken from Patent Application Number: 12552013,

"Hybrid Terrain -Adaptive Lower-Extremity Systems".

The main variables that we need to estimate to use the algorithm are orientation, O^{ω}_{ankle}, position, p^{ω}_{ankle}, and velocity, v^{ω}_{ankle}.

The orientation, O^{ω}_{ankle}, is represented by either a quaternion or a 33 rotation matrix that defines the orientation of the local frame attached to the ankle joint in relation to the world frame that is defined by gravity, $\vec{g}$.

The ankle joint is defined to be at the center of the ankle joint axis of rotation, while the orientation is attached to the lower leg shaft. After defining these points, the position of the joint center, along with, the velocity and acceleration are computed.

In this thesis, it is important to numerically integrate so that we can obtain a position of the ankle after heel-strike. To do this we need to remove the effects of scale, drift and cross-coupling with the world-frame orientation, from the velocity and position estimates that are introduced by integrating the accelerometer and rate-gyro signals.

The correction comes in the form of a zero-velocity update that averages over a short period of time during controlled dorsiflexion. The IMU measurements,a^{IMU}, are digitized in MATLAB and the ankle joint acceleration is derived using the following rigid body equation,

$$a^{IMU}_{ankle} = a^{IMU} + \vec{\omega} \times \vec{\omega} \times \vec{r}^{IMU}_{ankle} + \vec{\omega}\vec{r}, \tag{7.1}$$

where $\vec{\omega}$ and $\vec{\dot{\omega}}$ are the angular velocity and the angular acceleration in the IMU frame.

Equation 7.1, can be solved by using numerical integration with the following constraints,

$$\hat{\Phi}^{w}_{ankle} = \hat{\Omega}^{w}(\hat{\omega})\hat{\Phi}^{w}_{ankle} \tag{7.2}$$

$$\hat{v}^{w} = \hat{a}^{w}_{ankle} - [0, 0, g]^{T} \tag{7.3}$$

$$\hat{p}^{w}_{ankle} = \hat{v}^{w}_{ankle} \tag{7.4}$$

$$\hat{\Phi}^{w}_{foot} = \hat{\Phi}^{w}_{ankle}\hat{\Phi}^{ankle}_{foot} = \hat{\Phi}^{w} Rotation_{x}(\hat{\Omega}) \tag{7.5}$$

Then, this becomes,

$$\hat{v}^{w}_{heel} = \hat{v}^{w}_{ankle} + \hat{\Omega}^{w}\hat{\Phi}^{w}_{ankle}[\hat{\Omega}, 0, 0]^{w} r_{heel-ankle} \tag{7.6}$$

$$\hat{v}^{w}_{toe} = \hat{v}^{w}_{ankle} + \hat{\Omega}^{w}\hat{\Phi}^{w}_{ankle}[\hat{\Omega}, 0, 0]^{w} r_{toe-ankle} \tag{7.7}$$

$$\hat{p}^{w}_{heel} = \hat{p}^{w}_{ankle} + r^{w}_{heel-ankle} \tag{7.8}$$

$$\hat{p}^{w}_{toe} = \hat{p}^{w}_{ankle} + r^{w}_{toe-ankle} \tag{7.9}$$

$$r^{w}_{heel-ankle} = {}^{foot}\hat{\Phi}^{w}_{foot}(r_{heel} - r_{ankle}) \tag{7.10}$$

$$r^{w}_{toe-ankle} = {}^{foot}\hat{\Phi}^{w}_{foot}(r_{toe} - r_{ankle}) \tag{7.11}$$

In the above the matrix, $\hat{\Phi}$, can be used interchangeably with the orientation matrix, O^{w}_{IMU}.

Finally, the ankle joint velocity and position are derived from between the last, i^{th}, zero-veloicty update to the current moment according to the following equations,

$$v^{w}_{ankle}(t) = \int_{ZAUP(i)}^{t} (O^{w}_{IMU}) a^{IMU}_{ankle} dt \tag{7.12}$$

$$v^{w}_{ankle}(t) = \int_{ZAUP(i)}^{t} v^{w}_{ankle} dt, \tag{7.13}$$

where $p^{w}_{ankle}(t = ZVUP(i))$ is reset to zero for all i.

The accuracy of this method depends on the time over which the silent period is averaged and the thresholds used during that measurement. The designers of the iWalk ankle used logs of internal measurement unit data acquired from the IMU that was onboard the robotic ankle, and that the accelerations measured on the ankle in the z-direction (the direction of gravity) was about 1g. This combined with the ankle being in a controlled dorsiflexion state (the loading period during walking) along with the variance of the z-acceleration less than an experimental threshold of $0.005g^2$ suggested that the ankle was stationary and rotating about the ankle joint.

By using knowledge about the ankle joint and accelerations a reliable quiet period

can be approximated on this part of the foot that is co-located with an IMU. It is from these information that a zero-velocity update can be performed on successive gait cycles.

Due to the nature of walking a quiet stationary period almost always exists in a controlled dorsiflexion state. Even while walking over varying terrain a quiet control dorsiflexion state exists. This is due to the needs of the body to propel itself forward requiring the body to compress like a spring and rotate over the ankle joint.

During each of the zero-velocity update, three terms are evaluated to correct for changes in the pose of the ankle. The $\delta\theta_x$ of the world frame z-axis about the x-axis, that is the vector aligned with the ankle joint axis of rotation during the zero-velocity update during the previous step; the tilt, $\delta\theta_y$ of the world frame z-=axis about the y-axis; and the IMU scaling along the vertical axis, δg. From these values the post of the ankle is corrected, since the ankle is a rigid body moving through R^3.

When calculating the orientate, velocity and position integration, a sensitivity matrix, $M(t)$ is calculated that relates the velocity error that would be introduced by the vector of errors, $\alpha = [\delta\theta_x\ \delta\theta_y\ \delta g]^T$.

Formally, this relationship is,

$$M(t) = \frac{\delta}{\delta\alpha}(O^w_{IMU}\alpha^{IMU}_{ankle}),$$

that can be numerically integrated to generate the overall terminal velocity sensitivity, M^*,

$$M^* = \int_{ZVUP_{i-1}}^{ZVUP} {}_iM(t)dt.$$

From this value we can now update a Kalman Filtering algorithm that uses the Penrse psuedo-inverse, M^{*-1}, which can be included in the optimal innovations gail, K^* in the optimal linear feedback algorithm.

To actually use this algorithm the errors have to put back into the algorithm to update further estimates of pose and positions. Given that we know the zero-velocity update at a given step, i, the value of α would be determined by,

$$\alpha = M^{*-1} v^w_{ankle}(ZVUP_i),$$

where the innovations corrector vector is given by α. Since this is a physical system, part of the non-zero velocity results partly from noise in the accelerometers and angular rate measurements, so that not all of the correction, α, is applied.

To account for this a scaling factor is introduced that scales the filtering contestant, k, that depends on the magnitude of the noise in the system. From this a new orientation matrix, O^w_{ankle}, and gravity magnitude, g, are determined based on:

$$O^{w}_{ankle}(ZVUP^{+}_{i}) = O_x(-k\alpha(1))O_y(-k\alpha(2))^{w}_{ankle}O(ZVUP^{-}_{i}),$$

and

$$g(ZVUP^{+}) = g(ZVUP^{-}) - k\alpha(3),$$

where $O_x(tip)$ and $O_y(tilt)$ denote incremental rotations of the tip and tilt about the x and y axes respectively, and $ZVUP^{+}_{i}$ and $ZVUP^{-}_{i}$ denote the times after and before the $ZVUP$, respectively.

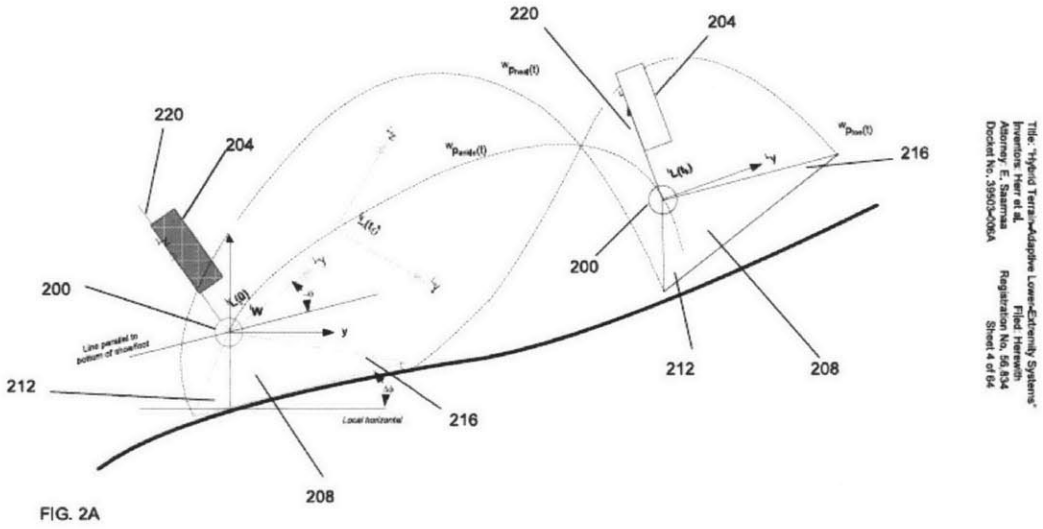

FIG. 2A

Figure 7-2: This is the schematic illustration a method for determining ankle joint, heel and toe trajectories of a prosthetic ankle.

Figures

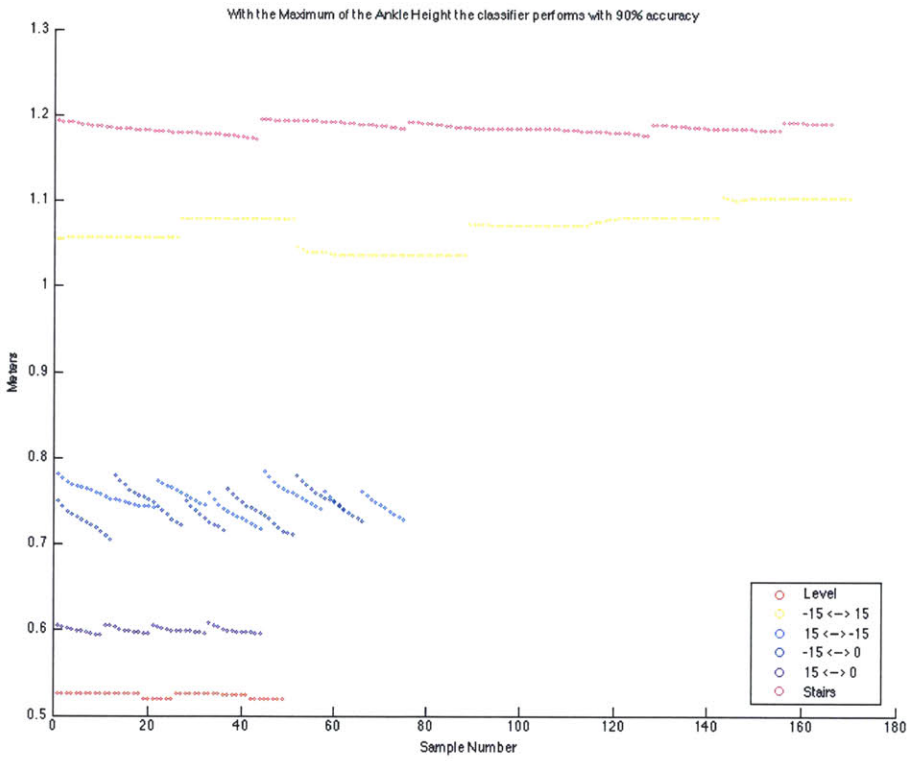

Figure 7-3: The first feature, of the two that comprise 100% accuracy, accounts for about 90% of the classification power of the algorithm. This is a large reduction and can be visualized by looking at the feature itself. The maximum height of the ankle in each extraction window separates almost all of the conditions except two which tend to overlap. The second feature teases out the difference between these two conditions.

EMG Channel Table (1 - 16)		
S1	S2	S3
Right Medial Gastroc	Right Medial Gastroc	Right Medial Gastroc
Left Medial Gastroc	Left Medial Gastroc	Left Medial Gastroc
Right Tibialis Anterior		Right Tibialis Anterior
Left Tibialis Anterior	Left Tibialis Anterior	Left Tibialis Anterior
Right Bicep Femoris	Right Bicep Femori	Right Bicep Femoris
Left Bicep Femoris	Left Bicep Femoris	Left Bicep Femoris
Right Rectus Femoris	Right Rectus Femoris	Right Rectus Femoris
Left Rectus Femoris	Left Rectus Femoris	Left Rectus Femoris
Right Semitend	Right Vastus Laterlis	Right Adductor Magnus
Left Semitend		Left Adductor Magnus
Right Vastus Lateralis	Right Semitend.	Right Vastus Lateralis
Left Vastus Lateralis	Left Semitend	Left Vastus Lateralis
Right Gluteus Maximus	Right Glute Maximus	Right Vastus Lateralis
Left Gluteus Maximus	Right Glute Maximus	Left Vastus Lateralis
	Right Tibialis Anterior	Right Gluteus Maximus
	Left Tibialis Anterior	Left Gluteus Maximus

EMG Channel Table (1 - 16)	
S4	S5
Right Medial Gastroc	Right Medial Gastroc
Left Medial Gastroc	Left Medial Gastroc
Right Tibialis Anterior	Left Tibialis Anterior
Right Bicep Femoris	Right Tibialis Anterior
Left Bicep Femoris	Right Bicep Femoris
Right Rectus Femoris	Left Bicep Femoris
Left Rectus Femoris	Left Rectus Femoris
Right Vastus Lateralis	Right Rectus Femoris
Left Vastus Lateralis	Right Adductor Magnus
Right Vastus Lateralis	Left Adductor Magnus
Left Vastus Lateralis	Left Vastus Lateralis
Right Adductor Magnus	Right Vastus Lateralis
Right Glute Max	Left Vastus Lateralis
Left Glute Max	Right Vastus Lateralis
Left Adductor Magnus	Right Gluteus Maximus
	Left Gluteus Maximus

Table 7.1: The EMG electrode recording sites varied little between subjects. Though on occasion some refinements were made to the number of the electrodes to improve the signal. This did not reveal any change in the overall influence of EMG as compared with intrinsic sensing.

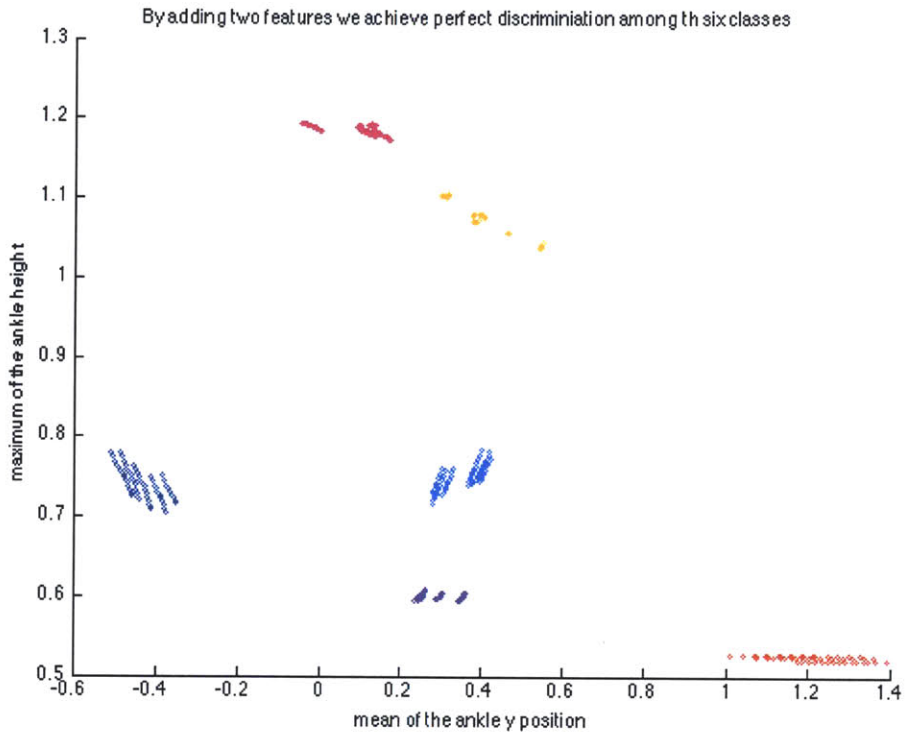

Figure 7-4: The two features extracted for the S1 A were able to perfectly discriminate between 6 different conditions. The power of this method lies in the nature of the features that use the maximum, mean, and minimum values of the height and forward distance in the classifier.

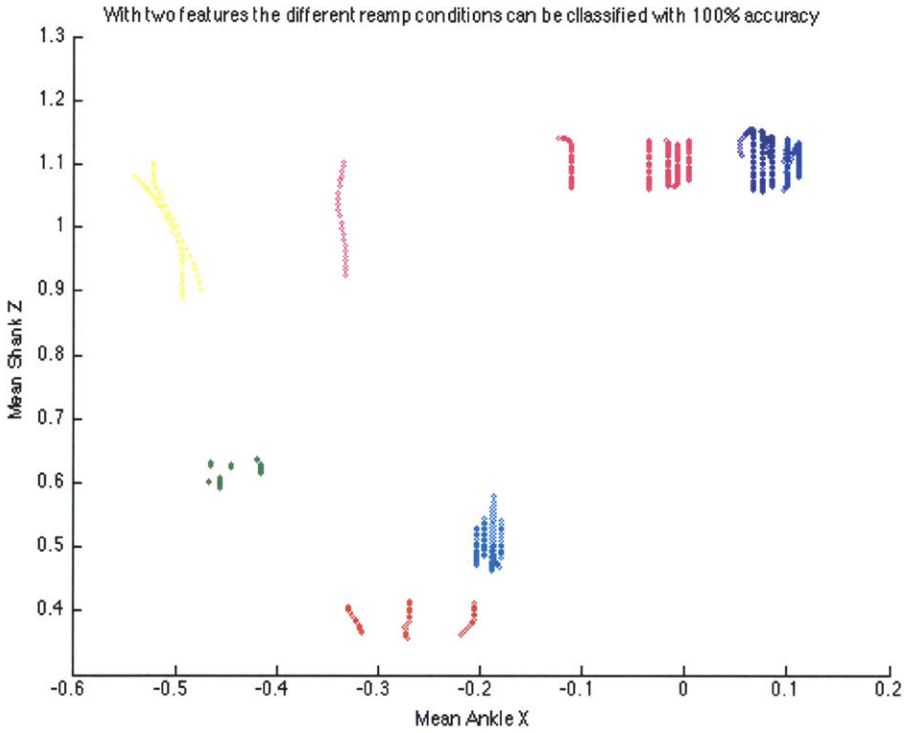

Figure 7-5: As in the case of S2 A the resultant feature space of 100% is well separated between clusters.

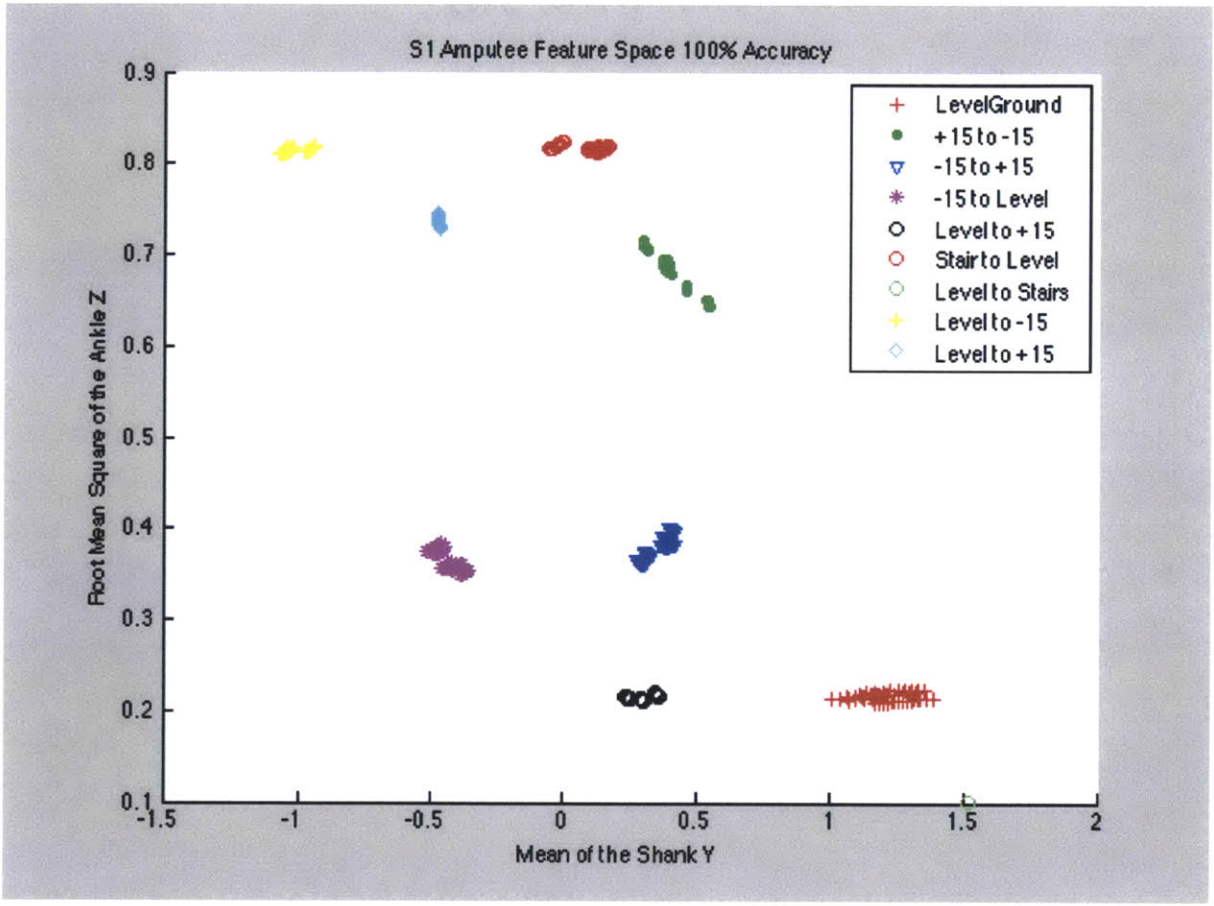

Figure 7-6: The feature space of the first amputee subject.

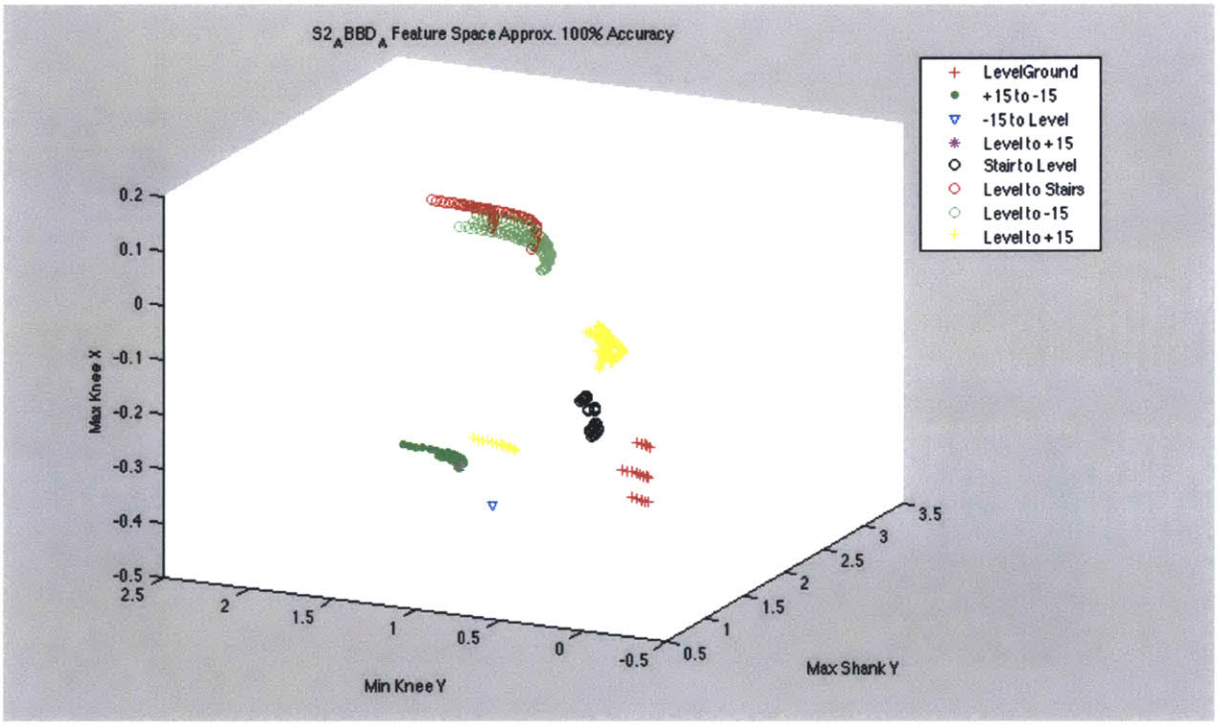

Figure 7-7: The feature space of the second amputee subject.

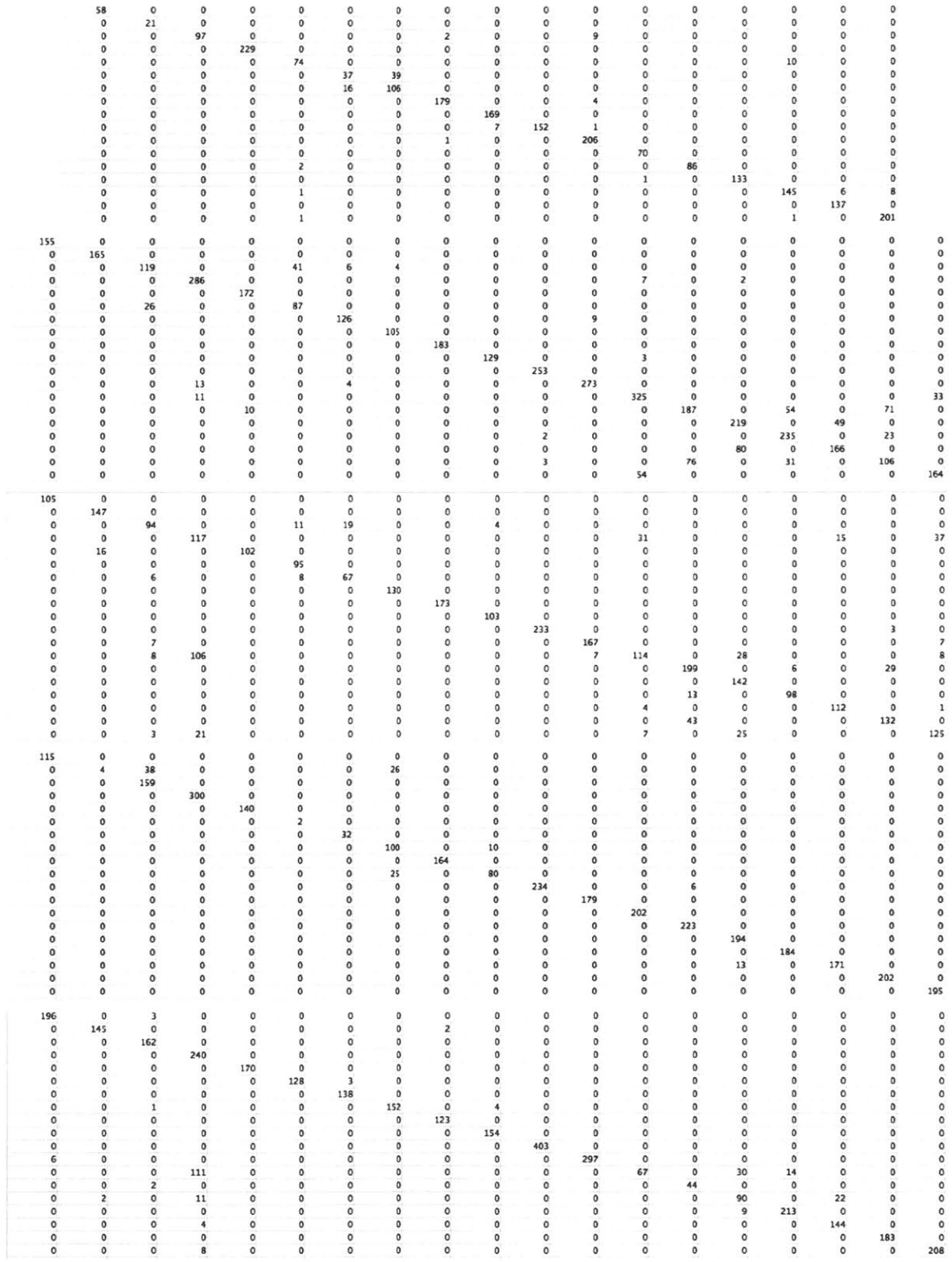

Figure 7-8: Each figure contains the confusion matrix from S1-S5 in order. Note that the matrix for S1 has only 17x17 entries in it's confusion matrix. This is due to experimental error where the stairs condition was corrupted. All other trials contain stairs as part of their 19 transitions.

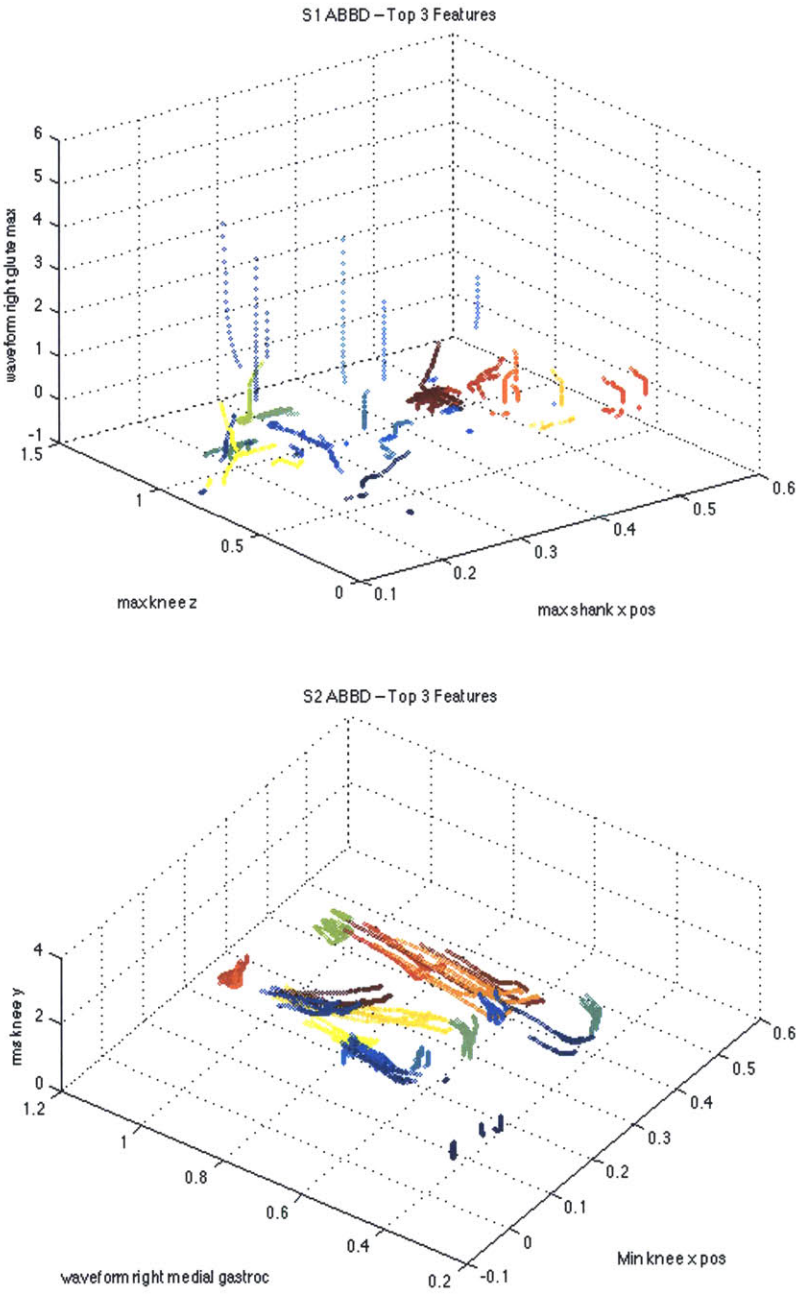

Figure 7-9: The first two feature spaces of subject S1 and S2. Shown are the top 3 features ordered by classification accuracy from X, Y, Z axes. Four out of five of the features for S1 were from intrinsic sensors and three out of five were from intrinsic sensors for S2.

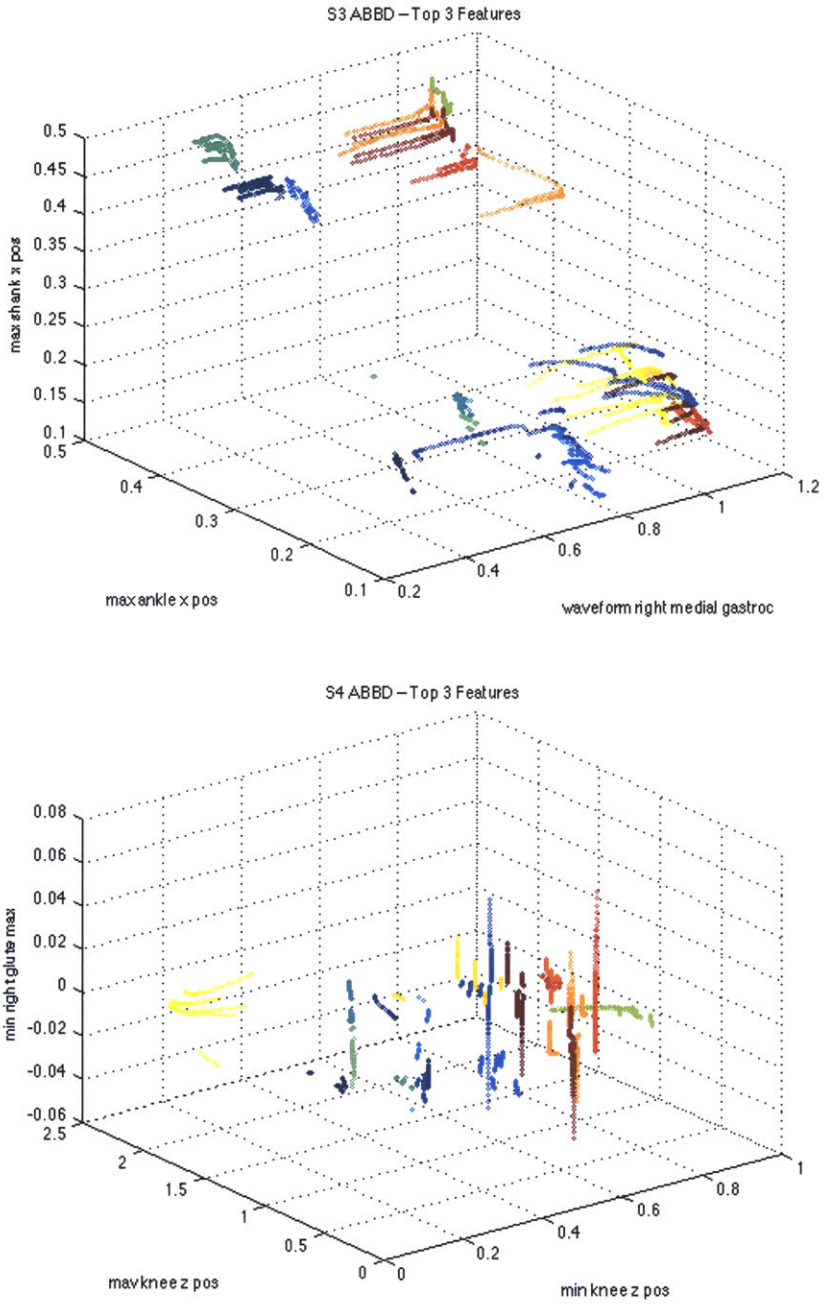

Figure 7-10: The next set of feature spaces of subject S3 and S4. Shown are the top 3 features ordered by classification accuracy from X, Y, Z axes. Two out of six features for S3 were from intrinsic sensors and three out of four features were from intrinsic sensors.

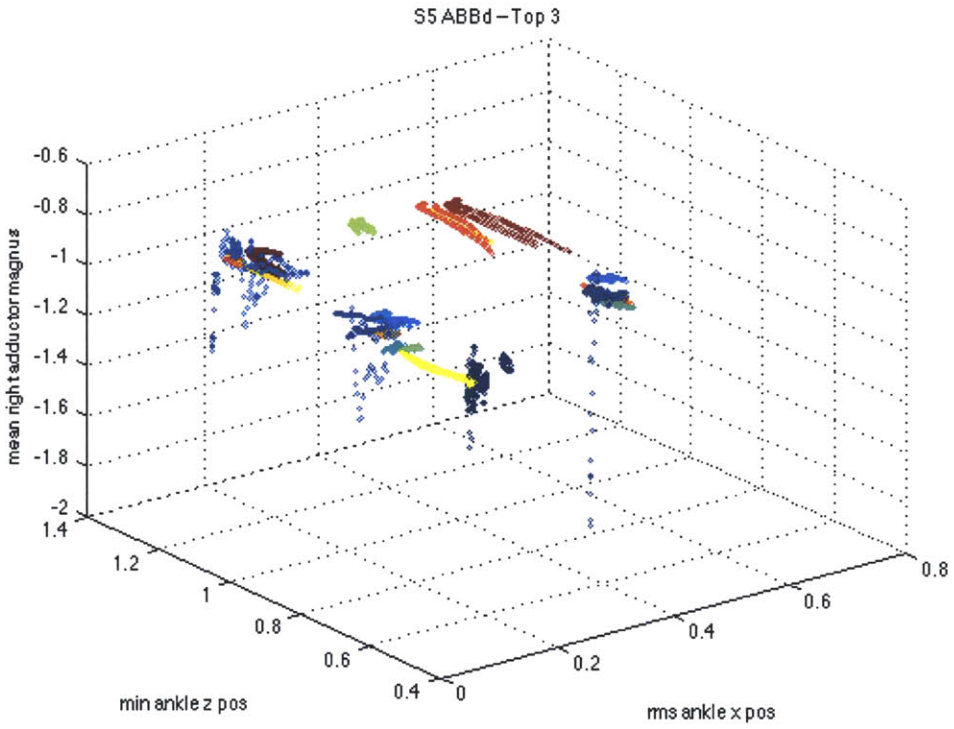

Figure 7-11: The next set of feature spaces of subject S5. Shown are the top 3 features ordered by classification accuracy from X, Y, Z axes. Three out of 4 features were from intrinsic sensors with S5.

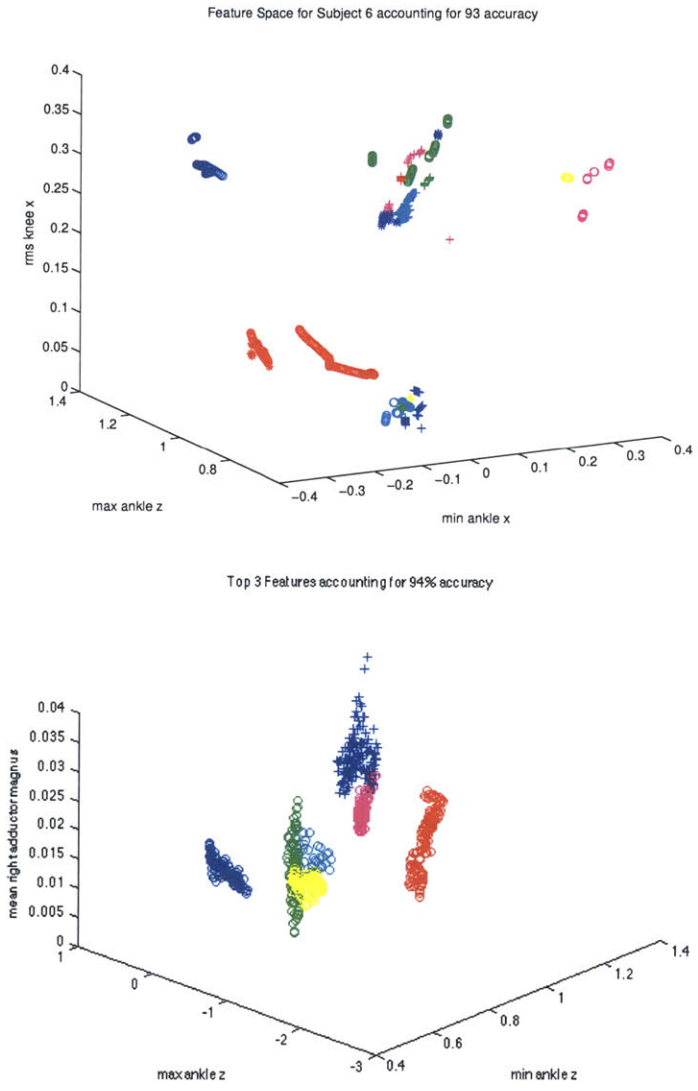

Figure 7-12: The final set of feature spaces for subjects S6 and S7. Four out of four sensors were from intrinsic sensors with S6 and three out of four were from for S7. The seven able-bodied subjects their associated feature spaces. Note that all the feature spaces shown here *do not* represent 100% classification accuracy. However, despite being below 100% there is already significant separation in most cases among classes with only three features.

Accuracy	Feature Number	Feature Type	Source
0.513 —	44	mean	knee z
0.696 —	33	mean	knee y
0.748 —	21	min	ankle z
0.836 —	25	autoregressive coef 3	knee y
0.878 —	37	rms	knee z
0.921 —	16	zcs	ankle z
0.937 —	11	mean	ankle y
0.969 —	20	max	ankle z
0.977 —	25	autoregressive coef 3	knee y
0.990 —	40	waveform	knee z

Figure 7-13: Results for Subject 1 using sensors and measuring heights and translations in the saggital plane.

Accuracy	Feature Number	Feature Type	Source
0.501 —	43	min	knee z
0.592 —	10	min	ankle y
0.744 —	15	rms	ankle z
0.865 —	32	max	knee y
0.920 —	16	mav	ankle z
0.960 —	37	rms	knee z
0.955 —	1	autoregessive coef 1	ankle y
0.965 —	4	rms	ankle y
0.976 —	5	mav	ankle y
0.988 —	26	rms	knee y

Figure 7-14: Results for Subject 2 using sensors and measuring heights and translations in the saggital plane.

Accuracy	Feature Number	Feature Type	Source
0.446 —	20	max	ankle z
0.556 —	4	rms	ankle y
0.620 —	31	max	knee y
0.656 —	9	max	ankle y
0.734 —	42	max	ankle z
0.761 —	1	autoregressive coef 1	ankle y
0.804 —	15	rms	ankle z
0.815 —	16	mav	ankle z
0.829 —	5	mav	ankle z
0.842 —	2	autoregressive coef 2	ankle y
0.838 —	3	autoregressive coef 3	ankle y
0.859 —	11	mean	ankle y
0.869 —	25	autoregressive coef 3	knee y
0.889 —	27	mav	knee y
0.904 —	22	mean	ankle z
0.911 —	14	autoregressive coef 3	ankle z
0.920 —	7	ssc	ankle y
0.941 —	44	mean	knee z
0.950 —	17	ssc	ankle y
0.947 —	6	zcs	ankle y
0.959 —	8	waveform	ankle y

Figure 7-15: Results for Subject 3 using sensors and measuring heights and translations in the saggital plane.

Accuracy	Feature Number	Feature Type	Source
0.484	11	mean	ankle y
0.654	9	max	ankle y
0.789	20	max	ankle z
0.919	32	min	knee y
0.949	29	mav	ankle z
0.971	21	min	ankle z
0.985	26	rms	knee y

Figure 7-16: Results for Subject 4 using sensors and measuring heights and translations in the saggital plane.

Accuracy	Feature Number	Feature Type	Source
0.44	31	max	knee y
0.571	9	max	ankle y
0.603	20	max	ankle z
0.659	5	mav	ankle y
0.743	33	mean	knee y
0.809	4	rms	ankle y
0.836	10	min	ankle y
0.866	22	mean	ankle z
0.895	43	min	knee z
0.919	27	ssc	knee y
0.931	40	waveform	knee z
0.938	1	ar coef 1	ankle y
0.945	32	min	knee y

Figure 7-17: Results for Subject 5 using sensors and measuring heights and translations in the saggital plane.

Accuracy	Feature Number	Feature Type	Source
0.472	3	ar 3	ankle y
0.548	9	max	ankle y
0.699	5	mav	ankle y
0.786	43	min	knee z
0.843	26	rms	knee y
0.902	10	min	ankle y
0.933	17	mav	ankle z
0.952	34	ar 1	knee z

Figure 7-18: Results for Subject 6 using sensors and measuring heights and translations in the saggital plane.

Accuracy	Feature Number	Feature Type	Source
0.55	20	max	ankle y
0.64	41	waveform	knee z
0.701	32	min	knee y
0.74	14	ar 3	ankle z
0.773	28	mav	knee y
0.78	1	ar 1	ankle y
0.794	9	max	ankle y
0.812	10	min	ankle y
0.837	11	mean	ankle y
0.86	15	rms	ankle z
0.873	33	mean	knee y
0.905	43	min	knee z
0.915	36	ar 3	knee y
0.93	44	mean	knee z
0.941	18	waveform	ankle z
0.952	31	max	knee y

Figure 7-19: Results for the Subject 7 using sensors and measuring heights and translations in the saggital plane.

Bibliography

[1] W.C. Flowers, "A Man-Interactive Simulator System for Above-Knee Prosthetics," PhD dissertation, Dept. Mech. Eng., MIT, Cambridge, MA, 1972.

[2] Hargrove, L.J. and Scheme, E.J. and Englehart, K.B. and Hudgins, B.S., "Multiple Binary Classifications via Linear Discriminant Analysis for Improved Controllability of a Powered Prosthesis", IEEE Trans. on Neural Systems and Rehab. Eng., 2010.

[3] He Huang and Kuiken, T.A. and Lipschutz, R.D., "A Strategy for Identifying Locomotion Modes Using Surface Electromyography", IEEE Trans. on Biomed. Eng., 2009.

[4] R. Psonak, "Transfemoral prosthetics", in Orthotics and Prosthetics in Rehabilitation, M. M. Lusardi and C. C. Nielsen, Eds. Boston, MA: Butterworth-Heinemann Publications, 2000.

[5] Au S. K. and Berniker, M., and Herr, H. "Powered ankle-foot prosthesis to assist level-ground and stair-descent gaits", Neural Networks vol. 21, pp.654-666, 2008.

[6] D. Jin, J.Yang, R. Zhang, R.Wang, and J. Zhang, "Terrain identification for prosthetic knees based on electromyographic signal features", Tsinghua Sci. Technol., vol. 11, pp. 7479, 2006.

[7] L. Peeraer, B. Aeyels, and G. Van Der Perre, Development of EMG based mode and intent recognition algorithms for a computer-controlled above-knee prosthesis, J. Biomed. Eng., vol. 12, pp. 178-182, 1990.

[8] R. Psonak, Transfemoral prosthetics, in Orthotics and Prosthetics in Rehabilitation, M. M. Lusardi and C. C. Nielsen, Eds. Boston, MA: Butterworth-Heinemann Publications, 2000.

[9] T. W. Williams III, Practical methods for controlling powered upperextremity prostheses, Assist. Technol., vol. 2, pp. 318, 1990.

[10] P. A. Parker and R. N. Scott, Myoelectric control of prostheses, Crit. Rev. Biomed. Eng., vol. 13, pp. 283-310, 1986.

[11] B. Hudgins, P. Parker, and R. N. Scott, A new strategy for multifunction myoelectric control, IEEE Trans. Biomed. Eng., vol. 40, no. 1, pp. 82-94, Jan. 1993.

[12] K. Englehart and B. Hudgins, A robust, real-time control scheme for multifunction myoelectric control, IEEE Trans. Biomed. Eng., vol. 50, no. 7, pp. 848 - 854, Jul. 2003.

[13] T.R. Farrell and R.F. Weir, "The optimal controller delay for Myoelectric Prostheses", IEEE Trans. Neural Systems and Rehab. Eng., vol. 15, no. 1, pp. 111-118

[14] D. L. Hall and J. Llinas, Introduction to Multisensor Data Fusion, Proc. of IEEE , Vol. 85, No. 1, pp. 6 - 23, Jan 1997.

[15] I. Guyon and A. Elisseefff, "An Introduction to Variable and Feature Selection", Journal of Machine Learning Research 3 2003 1157-1182 Submitted 11

[16] E. F. Delagi and A. Perotto, "Anatomic Guide for the Electromyographer The Limbs", 2d ed. Springfield, IL: Thomas, 1980.

[17] Frank Sup, Amit Bohara, Michael Goldfarb. "Design and Control of a Powered Transfemoral Prosthesis", The International Journal of Robotics Research, 2008.

[18] Hu, Mohammadreza Asghari Oskoei and Huosheng. "Myoelectric Control Systems - A Survey", Biomedical Signal Processing and Control, 2007.

[19] Edward A. Clancy, and Neville Hogan. "Probability Density of the Surface Electromyogram", IEEE Trans. on Biomed. Eng., 1999.

[20] Sawicki, GS., Ferris, DP. "A pneumatically powered knee-ankle-foot orthosis (KAFO) with myoelectric activation and inhibition", Journal of Neuroengineering and Rehabilitation, 2009.

[21] Gerald E. Loeb, Raymond A. Peck, William H. Moore, Kevin Hood. "BION system for distributed neural prosthetic interfaces", Medical Engineering and Physics, 2001.

[22] Scheinder, Patrick L., et al. "Accuracy and Reliability of 10 Pedometers for Measuring Steps over a 400-m Walk", Medicine and Science in Sports and Exercise, 2003.

[23] Miyazaki, S. "Long-term unrestrained measurement of stride length and walking velocity utilizing a piezoelectric gyroscope", IEEE Trans. on Biomed. Eng., 1997.

[24] K. Aminian Corresponding Author Contact Information, E-mail The Corresponding Author, a, B. Najafia, C. Blab, P. -F. Leyvrazc and Ph. Roberta. "Spatio-temporal parameters of gait measured by an ambulatory system using miniature gyroscopes." Journal of Biomechanics, 2002.

[25] Dejnabadi, H., et al. "Estimation and visualization of sagittal kinematics of lower limbs orientation using body-fixed sensors." IEEE Trans. on Biomed. Eng., 2006.

[26] Juan C. Moreno, a, , Eduardo Rocon de Limaa, Andrs F. Ruza, Fernando J. Brunettia and Jos L. Ponsa. "Design and implementation of an inertial measurement unit for control of artificial limbs: Application on leg orthoses." Sensors and Actuators B, 2006.

[27] P. Domingos, M. Pazzani, "On the Optimiality of the Simple Bayesian under Zero-One Loss." Machine Learning, 12, 103-130, 1997.

[28] Inbar, G., Paiss, O., Allin, J., Kranz, H., "Monitoring surface EMG spectral changes by the zero crossing rate", Medical and Biological Engineering and Computing, 1986.

[29] Hua, J., Tembe, W., Dougherty, E., "Performance of feature-selection methods in the classification of high-dimensional data", Pattern Recognition, 2008

[30] Liu et al., 2009 Liu, X., Zhou, R., Yang, L., Li, G., "Performance of various EMG features in identifying ARM movements for control of multifunctional prostheses", Proceedings of IEEE Youth Conference on Information, Computing and Telecommunication, pp. 287-290, 2009.